



**JNCC Report  
No. 649**

**An assessment of the value of natural capital in the protective  
service against coastal and inland flooding in the  
UK Overseas Territory of the British Virgin Islands**

**BVI Flood Resilience Modelling Tool - Technical Report**

**Jones, A., Trippier, B., Sym, E., Jones, G. & Wright, E.**

**September 2020**

**© JNCC, Peterborough 2020**

**ISSN 0963-8091**

**For further information please contact:**

Joint Nature Conservation Committee  
Monkstone House  
City Road  
Peterborough PE1 1JY  
<https://jncc.gov.uk/>

**This report should be cited as:**

Jones, A., Trippier, B., Sym, E., Jones, G. & Wright, E. 2020. An assessment of the value of natural capital in the protective service against coastal and inland flooding in the UK Overseas Territory of the British Virgin Islands: BVI Flood Resilience Modelling Tool - Technical Report. JNCC Report No. 649, JNCC, Peterborough, ISSN 0963-8091.

**JNCC EQA Statement:**

This report is compliant with the JNCC Evidence Quality Assurance Policy  
[jncc.gov.uk/about-jncc/corporate-information/evidence-quality-assurance/](https://jncc.gov.uk/about-jncc/corporate-information/evidence-quality-assurance/)

## Summary

This technical report outlines the modelling work conducted as part of a JNCC-led, CSSF-funded project aiming to assess the value of natural capital in providing protective services from storms and hurricanes in the British Virgin Islands (BVI). This project is a continuation of the CSSF Natural Capital in the Overseas Territories programme<sup>1</sup>: Natural Capital in the Caribbean and South Atlantic Overseas Territories: Valuation, Vulnerability and Monitoring Change.

The BVI are a Caribbean UK Overseas Territory that lie in the North Atlantic hurricane belt, and as a result are at constant risk from tropical storms and hurricanes during the yearly season, exemplified by the devastating impacts of Hurricanes Irma and Maria in 2017.

Two modelling frameworks were produced to assess how nature-based solutions can mitigate some of the risks associated with such storms; one to model inland run-off and flooding risk as a result of precipitation, and another to model flooding risk and marine risk as a result of storm surge. These frameworks were based on previous JNCC-contracted work with significant further development to both improve the models themselves and implement them in an automated and open-source workflow. An application was also developed in the R language with R Shiny to enable stakeholders in the BVI to run the models themselves in a simple and intuitive way, and to explore the effect on flooding risk of implementing different natural capital scenarios. A separate user guide has been produced to accompany the application.

Presented here are details of the two approaches and the application, as well as outputs produced by the models when run considering historic (Hurricanes Irma and Maria) and generic (tropical storm to Category 5) storm scenarios. Validation was conducted through two JNCC contracted projects: on the storm surge model using post-Irma and Maria damage estimates for the BVI (Williams *et al.* 2018), and for the inland flooding model by comparing modelled outputs to those produced as case studies for the BVI by a 2D hydrological model (Bray *et al.* 2019). Additionally, we present results of a simple assessment of the risk mitigation provided by natural capital, by comparing baseline flooding risk from precipitation and storm surge to the risk when changes to habitat and land cover are made, including the improvement and degradation of natural habitats and the removal of manmade impervious surfaces. The report ends by outlining the limitations and caveats of the models, and further work that may be conducted to improve them.

---

<sup>1</sup> <https://jncc.gov.uk/our-work/natural-capital-in-the-overseas-territories/>

# Contents

<b>1</b>	<b>Project introduction</b>	<b>1</b>
<b>2</b>	<b>Storm Surge Risk Modelling</b>	<b>2</b>
2.1	Introduction	2
2.2	Data sources and processing	2
2.2.1	Topographic layers	3
2.2.2	Habitat map and Manning's coefficients	3
2.2.3	Storm paths	3
2.3	Methods	4
2.3.1	Preparing the topography layers	4
2.3.2	Modelling fetch and continental shelf effects	5
2.3.3	Seabed friction layer	5
2.3.4	Cost distance analysis	6
2.3.5	Creating the total cost and risk layers	8
2.4	Results	9
<b>3</b>	<b>Inland Flood Modelling</b>	<b>14</b>
3.1	Introduction	14
3.2	Data sources	14
3.2.1	Topographic layers	15
3.2.2	Habitat map, erosivity and runoff values	15
3.2.3	Climate data	16
3.3	Methods	16
3.3.1	Storm precipitation	17
3.3.2	Habitat runoff and erosivity scores	18
3.3.3	Channel delineation and erosion risk	18
3.3.4	Travel time	20
3.3.5	Runoff and flooding risk	21
3.4	Results	21
<b>4</b>	<b>Combined Risk</b>	<b>26</b>
<b>5</b>	<b>Model Validation</b>	<b>28</b>
5.1	Storm surge model validation	28
5.2	Inland flood model validation	31
<b>6</b>	<b>Risk Modelling Application</b>	<b>32</b>
<b>7</b>	<b>Natural Capital Assessment</b>	<b>37</b>
7.1	Storm surge scenarios	37
7.1.1	Remove all the mangroves	37
7.1.2	Buffer the mangroves	38
7.1.3	Degrade the mangroves	38
7.2	Inland flooding scenarios	39

7.2.1	Convert all roads to grassland .....	39
7.2.2	Convert roads at elevations over 100m to grassland.....	39
7.2.3	Expand urban areas .....	41
<b>8</b>	<b>Limitations and Next Steps .....</b>	<b>43</b>
<b>9</b>	<b>References .....</b>	<b>46</b>

# 1 Project introduction

The 2017 hurricane season highlighted the urgent requirement to understand the role of natural capital in disaster resilience, to aid recovery in the British Virgin Islands (BVI). In this project, funded by the UK Government's Conflict, Stability and Security Fund (CSSF), JNCC supported the BVI Government by monitoring environmental change in the context of the role of natural capital in mitigating hurricane impacts, with the emphasis on supporting economic reconstruction, preparations for, and recovery from future hurricane impacts. The project aims to demonstrate the monetary and functional value of the natural environment to the BVI, including the importance of effective land use planning and restoration (nature-based solutions) to mitigate the effects of climate.

The project builds on previous work carried out under the programme 'Natural capital in the Caribbean and South Atlantic Overseas Territories: Valuation, vulnerability and monitoring change', by:

1. **Automating resilience modelling and carrying out improvements** including building a R Shiny tool to allow users to run the model based on future scenarios from tropical storm to hurricane events, including how to integrate future information from other data sources such as satellite data and hydrographic surveys;
2. **Disaster Charter Protocol and training** in collaboration with the UK Space Agency to enable British Virgin Islands to activate the Disaster Charter and access satellite data post-event if needed in the future;
3. **Generating an indicators framework** that will:
  - a. Develop long-term Environmental Sensitivity Indicators for use in new environmental legislation;
  - b. Develop disaster-related, short-term indicators to monitor post-hurricane impacts on the natural and built environment;
  - c. Supporting the use of the Defra 25 Year Environment Plan outcome indicators within the BVI.
4. **Training and capacity building** so that all relevant users can use the tools developed and delivered by the project.

This report will describe the technical detail around the development of the BVI Flood Resilience Modelling Tool (Point 1). This tool will be used by the BVI Government to understand the risks from flooding and enable users to generate scenarios to explore how these risks change in relation to potential land management decisions.

## 2 Storm Surge Risk Modelling

### 2.1 Introduction

Storm surge is a temporary change in ocean surface height occurring during hurricane conditions (Ellis & Sherman 2015) and represents one of the most dangerous meteorological effects resulting from a hurricane system in terms of loss of life (Rappaport 2014). Storm surge is caused primarily by the rotating winds of the hurricane which exert force on the surface of the water, pushing it in the wind's direction and creating a rising surge (which itself forces more water forwards to increase surge size), while a less significant proportion (10-15%) is caused by the lower pressure of a hurricane system relative to normal, acting to pull the water level upwards (Resio & Westerink 2008; World Meteorological Organization 2011). While these two factors provide a simple explanation of the origin of storm surge, it is, in reality, an incredibly complex meteorological phenomenon. The severity of surge is influenced by a large number of factors, including storm attributes (size, windspeeds, forward movement speed, angle of approach), local bathymetric and topological conditions, and land cover and its effects on surge attenuation (e.g. NOAA NHC 2020a; Ellis & Sherman 2015; World Meteorological Organization 2011; Irish *et al.* 2008; Resio & Westerink 2008; Barbier *et al.* 2013; Wamsley *et al.* 2010; Loder *et al.* 2009).

In the BVI, population concentration in coastal areas and the location of the Islands in the Atlantic hurricane belt makes storm surge a significant hazard (Bray *et al.* 2019). Hurricane Irma for example led to peak surge of over 6m (University of the West Indies 2017; Williams *et al.* 2018), damaging infrastructure and natural capital assets (Government of the Virgin Islands 2017). It is therefore important to understand how nature-based solutions may attenuate storm surge and improve resilience in the BVI, especially considering that extreme Atlantic hurricane seasons, such as that experienced during 2017, are likely to become more frequent under climate change (Lim *et al.* 2018). Here we further develop a simple cost-based model of marine and terrestrial risk from storm surge, based on previous JNCC-funded work (Williams *et al.* 2017). The model utilises a cost-distance analysis, which calculates the cumulative cost of travel from the storm path to at-risk marine and terrestrial areas, based on a cost landscape that includes information about topography (elevation, depth and slope), habitat, wind fetch distance, and offshore features. The automated model uses open source tools to refine the input layers, calculate the cost landscape and produce the final risk layers representing storm surge behaviour. While more complex hydrological models have previously been developed to assess and predict storm surge, such as the ADvanced CIRCulation (ADCIRC) coastal ocean model (Mattocks *et al.* 2006), the Coastal and Estuarine Storm Tide (CEST) model (Xiao *et al.* 2006, in Zhang *et al.* 2008), and the Sea, Lake and Overland Surge from Hurricanes (SLOSH) model (Jelesnianski *et al.* 1992) which is currently used in forecasting by the US National Hurricane Center (NOAA NHC 2020b), these were not implemented here. There are a number of reasons for this, but notably the desire to (a) keep the developed model and tools open source, (b) to minimise the technical and data requirements of the model, and (c) keep the model simple, R-integrated, and focussed on nature-based solutions; these meant that the cost-distance approach was maintained during this work.

### 2.2 Data sources and processing

All data were georeferenced to UTM 20N (ESPG:32620) and unless otherwise stated cropped to an area of interest extending 60km from the centroid of the BVI. Data processing and transformation was conducted in R version 3.6.1 (R Core Team 2019) calling on specialist functions from SAGA 2.3.2 64-bit version integrated through the 'RSAGA' package v1.3.0 (Conrad *et al.* 2015; Brenning *et al.* 2018), GDAL integrated through the 'gdalUtils'

package (Asher Greenberg & Mattiuzzi 2018) and GRASS 7.6.0 (Geographic Resources Analysis Support System) (GRASS Development Team 2019).

### 2.2.1 Topographic layers

A layer combining both terrestrial and bathymetric elevation was created by aggregating data from a number of sources. This layer was composed of a LIDAR-derived post-Irma and Maria topographic map of the BVI and some inshore waters created by the UKHO, with data gaps filled using UKHO survey data collected before hurricanes Irma and Maria. Where gaps in the data still remained over land, these were filled using data from the WorldDEM™ DTM (described in 3.2.1, see also Williams *et al.* 2017), and remaining gaps in the bathymetry were filled using GEBCO bathymetry data (GEBCO Compilation Group 2019). This created a “seamless” combined terrestrial-marine elevation layer. All raster manipulation was conducted in R using the ‘raster’ package v2.9-5 (Hijmans 2019).

The coastline boundaries layer was derived from OpenStreetMap (2019). The OpenStreetMap dataset for the BVI and the nearby USVI was downloaded, and manually edited in QGIS v3.4.5 (QGIS Development Team, 2018) to remove unnecessary features (line and point features, political features, *etc.*) leaving only a shapefile representing the coastlines of the BVI and nearby United States Virgin Islands (USVI). Anthropogenic coastal features (e.g. docks, piers) were left as part of the coastline, because of inconsistency in whether these were separate features or dissolved into the shapefile of the main island landmass.

### 2.2.2 Habitat map and Manning’s coefficients

A habitat map of the BVI and inshore waters was developed by Environment Systems Ltd as part of the vulnerability assessment of Anguilla and the BVI (Williams *et al.* 2018). To improve the representation of impervious road surfaces on this habitat map, data on the road networks present across the islands were obtained from OpenStreetMap (2019) and used to update the habitat map.

To represent the attenuation effects of these habitats on storm surge, Manning’s  $n$  coefficients were used to denote the surface roughness of the different habitat classes, being used to calculate drag and in turn impacting the cost of travel of storm surge over cells based on bed friction. These values were taken from previous storm surge modelling work (Zhang *et al.* 2013; Mattocks *et al.* 2006), with input sought for habitats not considered in these studies when required (Prager 1991, in Rosman & Hench 2011; Cialone & Smith 2007; Kraines *et al.* 1998; Bartleson 2004).

### 2.2.3 Storm paths

To create a storm path to act as an example for modelling purposes, we assumed a storm travelling along the East-South-Easterly prevailing wind direction for the BVI (Windfinder 2020). A storm path tracking ESE to WNW was created in QGIS using the Shape Tools plugin (Hamilton 2019), passing through the centroid of the islands. For the two modelled historical hurricanes, Irma and Maria, hurricane best track data were downloaded from NOAA’s National Hurricane Centre (NOAA NHC 2020c) and cropped to an area of interest extending 120km from the centre of the BVI, an extended AOI to account for Hurricane Maria’s distance from the BVI.

## 2.3 Methods

The storm surge model (Figure 1) was based upon a previous methodology deployed by Environment Systems Ltd (Williams *et al.* 2017), but further developed to better capture the impacts of the different factors effecting storm surge, and to show how risk may change with varying storm severity.

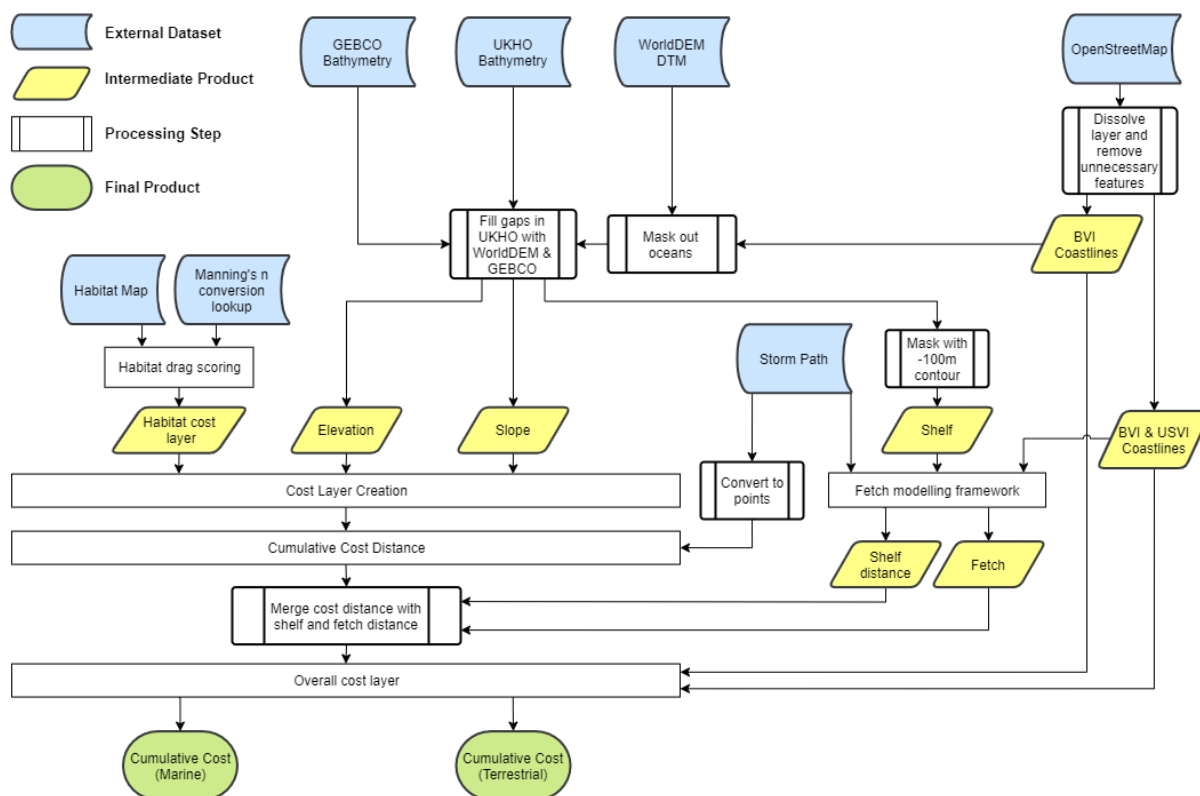


Figure 1: The storm surge model workflow.

### 2.3.1 Preparing the topography layers

Terrestrial elevation and terrestrial slope were included as factors in the cost-distance analysis based on the assumption that steeper slopes are more difficult for surge to overcome and higher elevations are more difficult for surge to reach. Therefore, increases in both factors are assumed to increase cost. Bathymetric depth and bathymetric slope were likewise included, as shallower shelves with shallower slopes produce increased surge (NOAA 2020a).

The elevation data were used to calculate a combined terrestrial-marine slope layer using the 'terrain' function in the 'raster' package, computing using the Horn (1981) algorithm for rough surfaces. The elevation layer was also used to derive the outline of the continental shelf, where any values shallower than -100m were reclassified as 'shelf' and deeper than -100m as 'open water'. The -100m depth threshold was chosen as a lower estimate of global average continental shelf depth (between -100 and -150m depths, Pinet 2003), and because visual assessments of the bathymetry layer found sharp drops in depth beyond this threshold, indicating that this was a suitable estimate for the separation between the shelf and open ocean.

### 2.3.2 Modelling fetch and continental shelf effects

Wind stress is the most significant force acting to create storm surge during a hurricane, and as such it is important to model factors affecting wind-wave behaviour. Here we included two measures of the effect of wind stress: a layer defining total wind fetch length (the uninterrupted over-ocean distance that wind has acted over to produce waves, following the previous model), and the uninterrupted distance the storm has travelled over the continental shelf, over which the fetch is effective at producing surge. Fetch acting over the open ocean has effects that we have assumed are likely to heighten risk, i.e. the production of swells and waves (Toffoli & Bitner-Gregersen 2017), and additionally represents an added measure of the level of exposure of coastal areas. As such, while only fetch acting over the shelf is effective at producing surge (World Meteorological Organization 2011), we chose in addition to include total fetch to capture the effect of exposure of islands close to the shelf edge.

The USGS method was used to model fetch (Rohweder *et al.* 2012), however rather than using the USGS ArcGIS plugin (Finlayson 2005; Rohweder 2012; Environmental Systems Research Institute 2020) as previously used in the method by Williams *et al.* (2017), the model was written in R, to ensure both that it could be automated successfully and also to utilise best our available data. Briefly, the USGS model calculates the angle of approach (relative to North) of the wind acting on an area and rotates a DTM raster layer of this area anticlockwise by the calculated angle. Doing so results in a raster where columns are aligned with wind direction, and rows can be counted to measure the distance covered by the fetch. When land is encountered (DTM values >0), the count is paused at elevations below 20m, maintaining the fetch value for the impacted coastline. When elevations exceed 20m the count is reset. This process is repeated a total of 9 times, once for the exact wind bearing, and once for eight more associated angles ( $\pm 3^\circ$ ,  $\pm 6^\circ$ ,  $\pm 9^\circ$ ,  $\pm 12^\circ$ ), to account for variability in wind direction (Rohweder *et al.* 2012). We reproduced the logic of this model in R, using a rasterised coastline shapefile layer instead of the DTM for analysis.

This code was then adapted to create a metric of distance travelled by a hurricane over the continental shelf. Shallow water continental shelf areas are significantly more important in effecting the surge created by a storm than open ocean areas, as only the fetch acting over shallow areas is effective at producing surge (World Meteorological Organization 2011), and therefore a wider and shallower shelf generally worsens generated surge. We therefore created a layer, representing the uninterrupted distance travelled by the hurricane over the continental shelf, based on the assumption that a storm that has covered greater distance over the continental shelf will have produced bigger surge and therefore will pose greater risk. This layer was calculated using the model produced for fetch, however rather than initiating the count of cumulative distance at the edge of the raster, the count started at the leading edge of the continental shelf, pausing when lowlands (elevation <20m) were encountered and resetting when either higher land (elevation >20m) or open water (elevation <-100m) was encountered.

### 2.3.3 Seabed friction layer

Coastal and inshore habitats (e.g. wetlands, reefs) have widely been observed to attenuate storm surge to varying degrees, although the exact dynamics are variable, owing to the attributes of the storm in question, and the quality and amount of habitat (with poor quality habitats sometimes increasing storm surge risk, Resio & Westerink 2008; Loder *et al.* 2009; Wamsley *et al.* 2010; Barbier *et al.* 2013; Pinsky *et al.* 2013; Möller *et al.* 2014). Here we took a simple approach to quantifying the effect of habitat on storm surge attenuation, using Manning's n coefficients which are a measure of surface roughness of habitats, denoting the amount of bed friction which would be expected to attenuate storm surge and therefore

reduce the expected risk to coastal regions (Mattocks *et al.* 2006; Westerink *et al.* 2006; Zhang *et al.* 2013). Values were retrieved from a number of sources (Table 1), and matched as far as possible to the habitat classifications used in the BVI habitat map. It should be noted that Manning's *n* values vary within habitat types based on the species composition and condition of the habitat, so the values used here should be considered approximations, and would be improved by studying the specific effects of the habitats in the BVI on water flow and drag.

The Manning's *n* coefficients were used to calculate the coefficient of drag exerted by bottom friction ( $C_f$ ) of different habitat classes, following Mattocks *et al.* (2006):

$$C_f = \frac{g \cdot n^2}{\sqrt[3]{H}}$$

Where *g* is acceleration due to gravity (9.81m/s<sup>2</sup>), *n* is the Manning's roughness coefficient, and *H* is the total height of the water column, including both bathymetric depth and additional surface elevation from surge. As surface elevation during the surge was unknown, a conservative estimate of a maximum of 20m was assumed, providing relative drag values per habitat type.

**Table 1:** The Manning's *n* coefficient values used for the BVI habitat classes, derived from Zhang *et al.* (2013).

No.	Habitat Class	Manning's coefficient	No.	Habitat Class	Manning's coefficient
1	Water	0.020	11	Scrub	0.050
2	Sediment	0.040	12	Rock	0.090
3	Reef <sup>1</sup>	0.100	13	Mixed Forest	0.100
4	Beach	0.040	14	Urban	0.100
5	Mangrove	0.100	15	Bare	0.020
6	Thicket	0.100	16	Evergreen Forest	0.110
7	Salt Pans	0.048	17	Agriculture	0.350
8	Drought Deciduous Scrub	0.050	18	Semi-Deciduous Forest	0.100
9	Salt Pond	0.048	19	Seagrass <sup>2</sup>	0.050

1. Reported values varied from 0.05 (Prager 1991, in Rosman & Hench 2011) to 0.25 (Cialone & Smith 2007). A conservative central value of 0.1 (Kraines *et al.* 1998) was used in modelling.
2. Chosen based on calculated Manning's *n* coefficient for *Ruppia maritima*, another aquatic grass-like vegetation (Bartleson 2004).

### 2.3.4 Cost distance analysis

Previous work utilised a cost distance analysis as a simple model to determine relative risk of onshore and offshore areas to storm surge (Williams *et al.* 2017). This analysis acts on a raster describing the cost landscape, where cell values represent the cost of theoretical travel through that cell. For each cell in the raster, the cumulative sum of the least-cost route to a selection of starting locations (in this case the path of the storm) is calculated. This results in an output raster where each cell's value is the lowest possible cumulative cost of

travel from that cell to the starting points. Applying this in the context of storm surge, cost can be thought of in terms of attenuation, where higher cost in a cell represents higher attenuation of storm surge, and therefore lower risk to cells beyond. To generate a layer describing the cost landscape of BVI relevant to storm surge, derived layers (elevation, slope, friction) were reclassified into layers representing their effect on cost. In the case of elevation and slope, this simply required rounding all values up to the nearest integer, with exact 0s in the slope layer being rounded up to 1, to avoid multiplication by 0 errors. No specific reclassification was required for the friction layer. All cost layers were masked such that values above 20m elevation were converted into NAs, with 20m being chosen as a conservative estimate of maximum surge height. Doing so prevents the cost distance analysis calculating a cumulative least cost that is not logical in the context of storm surge (e.g. surge travelling over areas of 100m elevation because it produces a lower cumulative cost).

The created cost layers were combined into an overall cost layer, with cost per cell to storm surge ( $C_{SS}$ ) calculated as:

$$C_{SS} = \frac{(E \cdot (S_t \cdot \alpha)) + (D \cdot (S_b \cdot \alpha) \cdot \beta) + (C_f \cdot \gamma)}{F_{SC}}$$

Where  $E$  = terrestrial elevation,  $S_t$  = terrestrial slope,  $\alpha$  = slope weighting factor,  $D$  = bathymetric depth,  $S_b$  = bathymetric slope,  $\beta$  = bathymetric weighting factor,  $C_f$  = drag coefficient,  $\gamma$  = friction weighting factor, and  $F_{SC}$  = storm category factor.

The factor  $\alpha$  was included to dampen the effect of the slope term, which could result in extremely high costs at large values when multiplied by elevation costs. The factor  $\beta$  acts to reduce the relative cost of bathymetric elevation and slope relative to terrestrial elevation and slope, based on the assumption that moving over large terrestrial elevations and slopes is more costly for surge than comparable bathymetry slopes and depths (e.g. that a cell containing a 90° slope at 10m elevation is more costly for surge to travel over than a cell containing a 90° slope at an elevation of -10m). The factor  $\gamma$  is intended to scale the friction coefficient values to a magnitude on a par with the costs seen in the elevation and slope layers, and the  $F_{SC}$  factor is a weighting factor to reduce cost (and therefore increase risk) in higher categories (Table 2). Category was chosen as the scaling factor to maintain consistency with the inland flooding model, and because increasing category results in increasing wind speeds and therefore, in theory, worse surge. However, numerous other factors affect surge, and it has been suggested that category is in fact a poor predictor of surge size, especially compared to factors such as storm size (Irish *et al.* 2008). We have assumed here that increasing category is linked to increases in other storm attributes (e.g. size), however storm attributes are not necessarily linked to storm category, and this should be kept in mind when implementing the model.

**Table 2:**  $F_{SC}$  values for different storm categories.

Storm Category	$F_{SC}$ Value
Tropical Storm	1.0
Category 1	1.1
Category 2	1.2
Category 3	1.3
Category 4	1.4
Category 5	1.5

The values for factors  $\alpha$ ,  $\beta$ ,  $\gamma$ , and  $\varepsilon$  (see 2.3.5 below) were chosen through sensitivity analysis, testing every combination of chosen testing values (Table 3). Additional values were tested in earlier iterations of the sensitivity analysis during model development, and the values tested in the final run represented those that proved most appropriate in previous tests. Each combination of parameter values was used in a version of the cost distance analysis (using the Hurricane Irma storm path). The outputs were then compared to extents of observed and potential damage on Virgin Gorda, Beef Island, and Anegada, following Hurricanes Irma and Maria (Williams *et al.* 2018). The percentage of these damaged areas modelled as Moderate, High, or Very High risk was assessed. Each test was also repeated, whilst excluding the cost attributed to elevation above 0m. This was to test the possibility that elevation was being overrepresented, both being a cost factor itself and correlated to an input to the friction equation. However, the sensitivity analysis found that model results were improved with terrestrial elevation included. Such a test was not conducted for bathymetry, despite it also being a factor in itself and an input to the friction equation, since in these two cases bathymetric depth have opposing effects: shallower depths increase the size of storm surge (World Meteorological Organization 2011), but bottom friction creates greater drag in shallow depths, leading to increased attenuation. Given that these two layers have opposing effects, we felt it was acceptable to include them in the model without conducting a sensitivity analysis similar to that of terrestrial elevation. Sensitivity analysis resulted in the final parameter values as seen in Table 3.

**Table 3:** Values tested in the sensitivity analysis for the three scaling factors, and the final value chosen for each as a result of the sensitivity analysis.

Factor	Tested Values	Final Value
$\alpha$	0.10; 0.25; 0.50	0.10
$\beta$	0.10; 0.25; 0.50	0.10
$\gamma$	600; 700; 800; 900; 1000	1000
$\varepsilon$	0.50; 0.75; 1.00	0.50

The cost distance analysis was conducted using the “r.cost” function in GRASS (Geographic Resources Analysis Support System) GIS 7.6 (GRASS Development Team 2019).

### 2.3.5 Creating the total cost and risk layers

The fetch and shelf distance layers were rescaled to make them of equal magnitude to the cumulative cost distance (the output of the cost distance analysis), first inversely rescaling them between 0 and 1 (such that maximum distance became 0 cost and minimum distance became 1 cost), then adding the layers, and finally rescaling this combined layer between 0 and the maximum cumulative cost distance of a Category 2 hurricane along the same path. This combined and rescaled fetch and shelf distance (*FSD*) was weighted based on a weighting factor  $\varepsilon$ , and added to the output of the cost distance analysis, the cumulative cost distance (*CD*), to provide a layer representing total cost ( $C_T$ ):

$$C_T = CD + FSD \cdot \varepsilon$$

The scaling factor  $\varepsilon$  was included here to modulate the relative effects of attenuation (cost distance) and propagation (fetch and shelf distance) on storm surge, and tested during the sensitivity analysis as before, using the values seen in Table 3.

Total cost ( $C_T$ ) was split into two layers representing marine and terrestrial risk and reclassified into 9 and 5 risk categories respectively. Cost boundaries for these risk categories were derived from quantile boundary values for a Category 2 hurricane following

the same track, with 9 quantiles being calculated for marine areas and 5 for terrestrial areas in a Category 2. Reclassification was conducted such that cells with high cost (values in the range of the highest quantile) were reclassified as the lowest risk, and vice versa. A Category 2 storm was chosen as a baseline as it represents an approximately mid-strength storm, but by choosing it over a Category 3 storm a conservative estimate of risk at higher storm categories is maintained.

## 2.4 Results

The storm surge modelling framework is best assessed when compared to the one historical estimate of storm damage to which we had access, as conducted during the sensitivity analysis. Overall, 94.4% of observed damaged area after Hurricanes Irma and Maria across the 3 test islands was modelled as Moderate, High, or Very High risk from Hurricane Irma (Figure 2) using this model (Beef Island = 91.0%, Anegada = 97.1%, Virgin Gorda = 95.3%). In total, 88.5% of potentially damaged area was modelled as Moderate to Very High Risk. Conversely, 50.4% of undamaged area was rated Moderate to Very High on Beef Island, 93.8% on Anegada, and 15.4% on Virgin Gorda. The differing rates of overestimation here are likely a result of the topography of the islands in question, with flatter islands more likely to have higher estimates of risk in areas which were not observed as damaged, as a result of the lower scaling factor associated with elevation cost. However, since we are favouring a risk-averse approach, overestimation in undamaged areas is preferable to underestimation in damaged areas (more information can be found in Section 5.1). Hurricane Maria (Figure 3) was not compared against the damage lines, as Hurricane Maria caused minor surge in comparison in the BVI (Pasch *et al.* 2019), though despite this the BVI is predicted by this model as being at high risk of storm surge from Hurricane Maria. This is most likely the simultaneous result of two factors, (a) the model outputs being self-referential, in that quantile values (and in turn risk categories) are generated by comparing the modelled storm to a Category 2 storm of the same path, which therefore means the much greater distance of Hurricane Maria from the BVI has little effect in altering terrestrial surge risk, and more importantly (b) the fact that the model is not a hydrological model, and does not capture the more nuanced effects of hurricane dynamics on storm surge.

Outputs for Category 1 (Figure 4) and Category 5 (Figure 5) storms are also presented below, and while visual assessment of the outputs indicates the model is performing as expected, a lack of ground truthing data leaves us unable to validate these outputs.

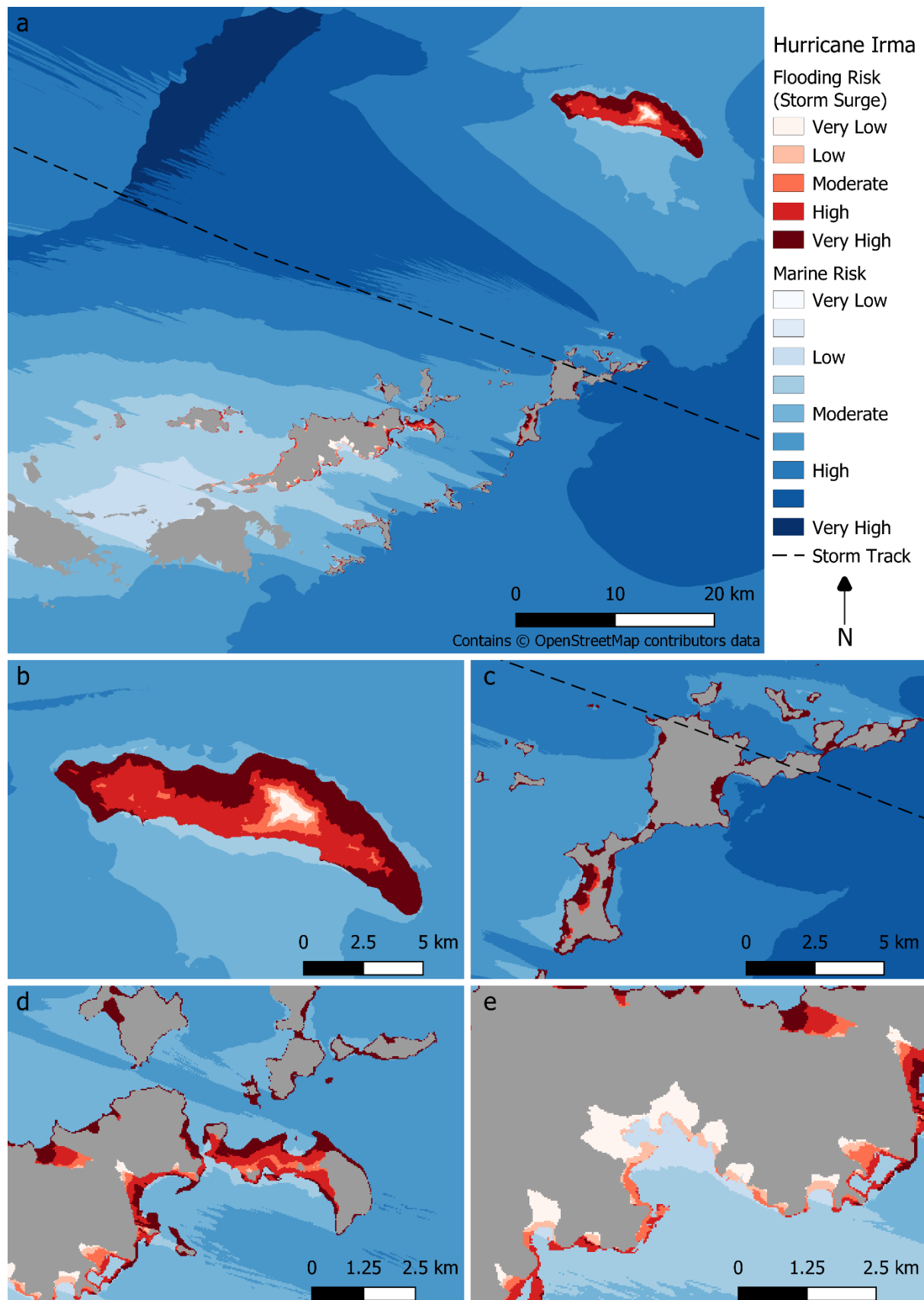


**Figure 2:** Modelled terrestrial flooding risk (red) and marine risk (blue) from Hurricane Irma for the British Virgin Islands (a). Detailed views of Anegada (b), Virgin Gorda (c), Beef Island (d), and Road Town (e) are provided.

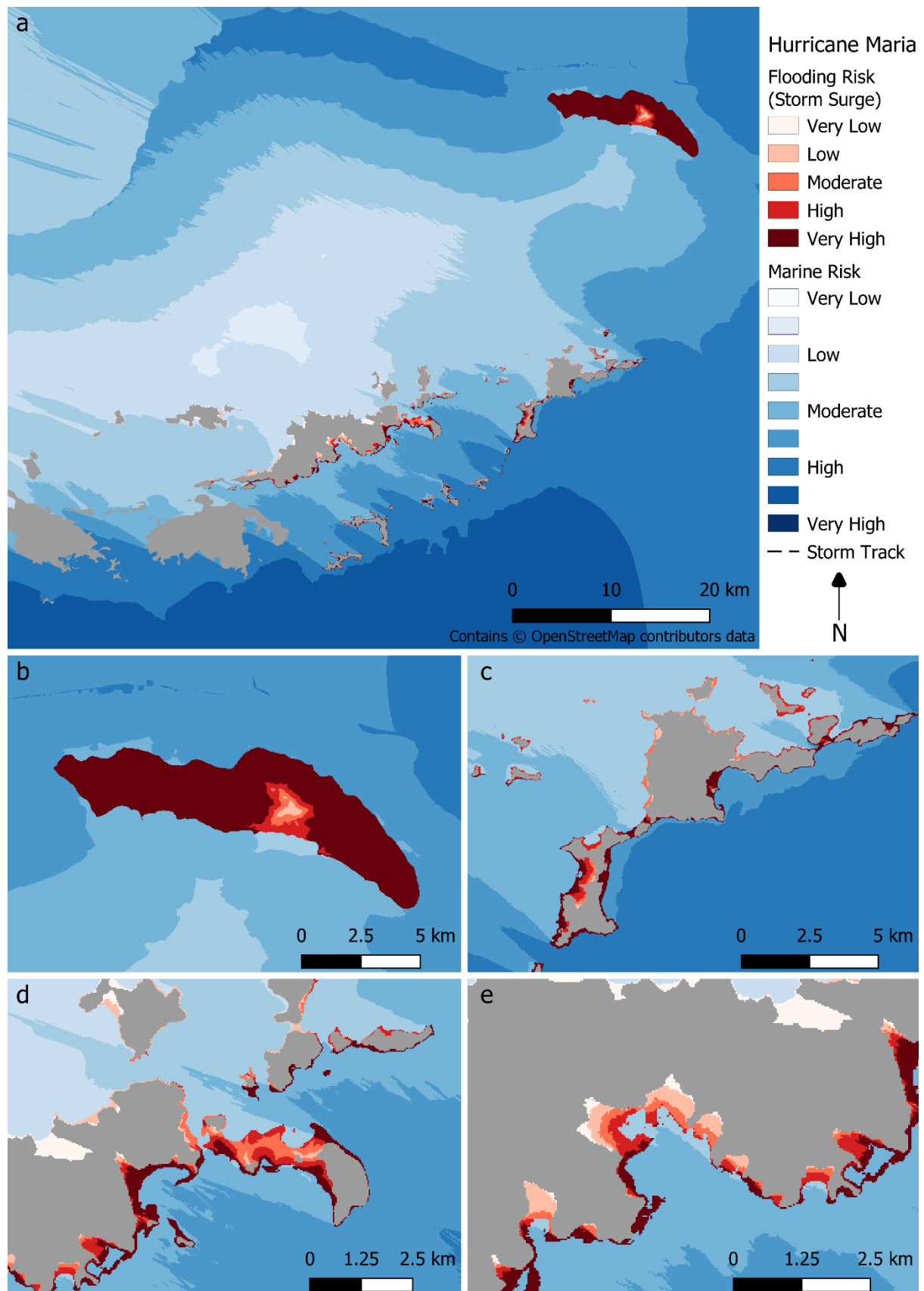


**Figure 3:** Modelled terrestrial flooding risk (red) and marine risk (blue) from Hurricane Maria for the British Virgin Islands (a). Detailed views of Anegada (b), Virgin Gorda (c), Beef Island (d), and Road Town (e) are provided.

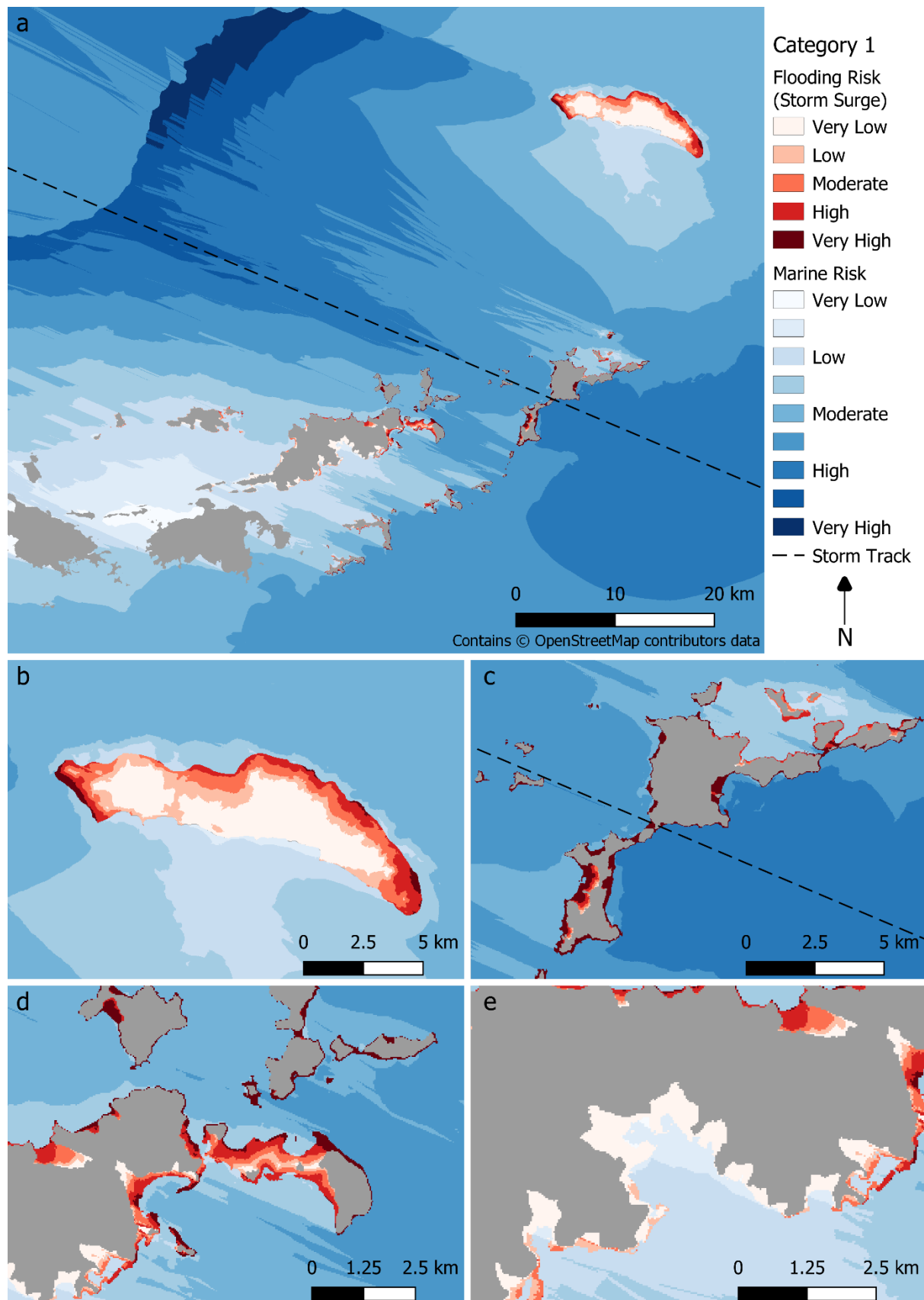


**Figure 4:** Modelled terrestrial flooding risk (red) and marine risk (blue) for the British Virgin Islands (a). Detailed views of Anegada (b), Virgin Gorda (c), Beef Island (d), and Road Town (e) are provided. This storm was modelled as a Category 1, with an ESE to WNW track (dashed line) passing through the centroid of the islands.

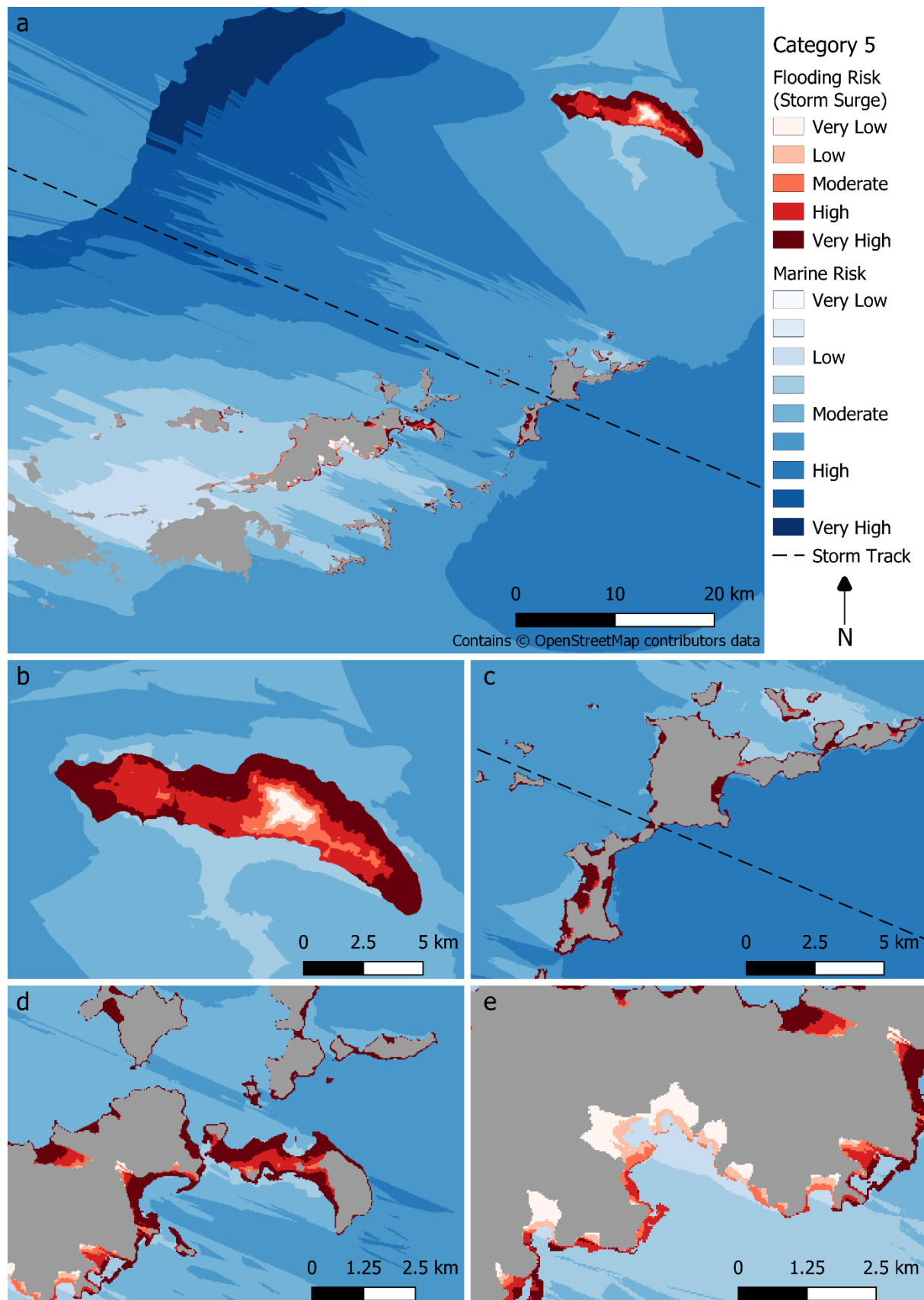


**Figure 5:** Modelled terrestrial flooding risk (red) and marine risk (blue) for the British Virgin Islands (a). Detailed views of Anegada (b), Virgin Gorda (c), Beef Island (d), and Road Town (e) are provided. This storm was modelled as a Category 5, with an ESE to WNW track (dashed line) passing through the centroid of the islands.

## 3 Inland Flood Modelling

### 3.1 Introduction

Extreme rainfall, particularly during storm events, has caused severe inland flooding in recent years across the British Virgin Islands (Bray *et al.* 2019). The BVI's steep topography channels runoff downstream into the low-lying coastal settlements, which can lead to rapid surface water accumulating in towns and cities, destroying homes and livelihoods. The small island communities sit in the Atlantic hurricane belt and are particularly vulnerable to hurricane events, exposing them to high windspeeds, precipitation and storm surge, with events having increased in frequency as a consequence of climate change (Williams *et al.* 2017). Therefore, careful risk mapping of areas likely to experience flood damage can help to inform at-risk areas and assess how nature-based solutions can help to alleviate risk.

Previous studies in the BVI assessing inland flooding have been conducted using a wide variety of modelling techniques, varying in their complexity, data requirements and informative capabilities. Bray *et al.* (2019) used the software 'InfoWorks' ICM (Integrated Catchment Model) to develop detailed 2D hydraulic models, predicting flood depths for various storm events and habitat scenarios. The models required high resolution data on elevation, buildings and land use, and pluvial hyetographs from previous rainfall storm events to create a triangular mesh of the land surface and produce output maps of likely flooding depths in major cities. In contrast, another study conducted for JNCC (Williams *et al.* 2017) developed a simplistic 1D inland flood model to demonstrate vulnerable areas in the UK Overseas Territories. This used a DTM layer, land cover map, and information on soil and geology to perform hydrographical analysis using SAGA (Conrad *et al.* 2015), a hydrological software incorporated into QGIS v3.4.5 (QGIS Development Team 2018). They developed maps of flood risk from both moving and standing water. The standing water risk was modelled from a 'hollows' layer, depicting where water is likely to pool during heavy rainfall, derived from elevation data. The moving water risk was modelled through delineating likely waterflow channels using the SCIMAP fine sediment erosion model (Reaney *et al.* 2011). These modelling approaches differ in their predictive abilities to describing patterns of floodwater during storm events, with the more complex hydrological models requiring a wider range of data inputs and knowledge to create and run the models.

As these are small island communities with limited data availability and analytical capabilities, this study aimed to develop an automated reproducible methodology, using open-source software, to provide an indication of which areas are likely to be threatened by flooding from precipitation during storm events. It was important to incorporate different storm patterns and characteristics to demonstrate how risk varies with different degrees of storm severity, and how anthropogenic impacts can lead to rapid movement of surface waters. Therefore, a simplistic risk model was developed using available data to predict the risk of an area experiencing high levels of runoff based upon the topography, land use, and maximum precipitation experienced during a storm. This was then masked to the likely flooding zones to identify regions at high risk of damage from flooding.

### 3.2 Data sources

All data were georeferenced to UTM 20N (ESPG:32620) and cropped to the area of interest. Data processing and transformation was conducted in R version 3.6.0 (R Core Team 2019), SAGA 2.1 64-bit version integrated through the 'RSAGA' package v.1.3.0 (Conrad *et al.* 2015; Brenning *et al.* 2018) and GDAL integrated through the 'gdalUtils' package (Asher Greenberg & Mattiuzzi 2018).

### 3.2.1 Topographic layers

The Digital Terrain Model (DTM) was derived by Environment Systems Ltd from a WorldDEM™ product of their AOI, which was mosaicked and reprojected from WGS84 into the local Transverse Mercator (UTM) (Williams *et al.* 2017). The DTM was resampled to 10m using the 'gdalUtils' R package 'gdalwarp' function, resampling using a cubic methodology (Asher Greenberg & Mattiuzzi 2018), and masked to the coastline boundaries layer to give the terrestrial elevation of the islands.

The coastline boundaries layer was derived from OpenStreetMap (2019), described in Section 2.2.1. These were then manually assessed to remove small jetties and islands from the coastline, as very small flat regions interfered with processes within the SCIMAP model causing errors when trying to plot the results. These were removed manually in QGIS v3.4.5 (QGIS Development Team 2018) to remove these object shapes and simplify the coastline boundaries layer.

### 3.2.2 Habitat map, erosivity and runoff values

The habitat map was developed by Williams *et al.* (2018), using segmentation and random forest modelling and assessed against ground truthing points from Kennaway *et al.* (2008). Data on the road networks present across the islands were obtained from OpenStreetMap (2019) and were used to update the habitat map, with roads being assigned the land class "urban". The final habitat layer was then rasterised at 30m spatial resolution.

The erosivity values for each habitat class were derived through literature reviews of case studies using SCIMAP (Sensitive Catchment Integrated Modelling and Analysis Platform) Fine Sediment Risk Model (Reaney *et al.* 2011) and the land cover risk weightings associated with different habitat classes (Perks *et al.* 2017). As SCIMAP has mainly been implemented to model catchments in Europe, these values were adjusted for the land classes present in the BVI.

The runoff values relate to the proportion of precipitation that falls on a habitat that is converted to runoff. These were obtained from guidance for using SCIMAP-Flood developed by Reaney and Pearson (2019) which looks to model natural flood risk from the rainfall and runoff generation patterns in the landscape, and spatially target flow-slowing natural management schemes. This risk-based approach assumed land cover to be the dominant factor in predicting runoff generation in the landscape and assigns relative values per land cover class. These were developed with UK hydrological catchments in mind, therefore these values were adjusted to be applicable to the habitat classes found in the BVI. Waterbodies and Inland rock were assigned the value of 1 as all the rainfall is assumed to be converted to runoff. This simplistic assignment of runoff values is limited as it is not accounting for spatial variation between habitats of the same type or considering the influence of soil type and depth upon the levels of infiltration.

Soils were not included in the analysis despite their importance to hydrological cycling. Comparisons of the Harmonized continental SOTER-derived database (SOTWIS) (ISRIC 2019) at a resolution of 30 arc seconds revealed little change between the islands in their parent material and dominant soil type (IB2-KSI – Chrtomi-Luvic Kastanozems), therefore this layer was not included in the analysis, however did provide an indication of the erodability of the underlying soil type present. It was also noted in Wood PLC's (2019) assessment of the territory that soils were thin on the islands lending to the steep topography being the main driver of erosion and rainfall conversion to runoff.

### 3.2.3 Climate data

To simulate risk during storms of different categories as defined by the Saffir-Simpson hurricane wind scale (SSHWS), climate data was collated from known storm events that have impacted the British Virgin Islands. Daily precipitation data were obtained from the 3B42 RT Derived Daily Product from the Tropical Rainfall Measuring Mission (TRMM), available through NASA's Giovanni data service (Huffman *et al.* 2014). This was obtained at 0.25 degree resolution for dates where tropical storms and hurricanes were known to impact the BVI based on records from the BVI's Department of Disaster Management (2019) through their online news feed and records available through the National Hurricane Center and Central Pacific Hurricane Center run by the National Oceanic and Atmospheric Administration (2020). The storm events included are shown below in Table 4.

**Table 4:** Storm events used to collate the maximum precipitation values for categories of storm as defined by the Saffir-Simpson hurricane wind scale (Department of Disaster Management, British Virgin Islands 2019; NOAA NHC 2020d).

Storm Category	Sustained Winds (mph)	Storm Events	Storm Date
Tropical storm	<74	Tropical Storm Karen	24/08/2019
		Tropical Storm Isaac	14/09/2018
		Tropical Storm Beryl	09/07/2019
Category 1	74-95	Hurricane Dorian	30/08/2019
		Hurricane Earl	30/08/2010
Category 2	96-110	-	-
Category 3	111-129	-	-
Category 4	130-156	-	-
Category 5	>157	Hurricane Maria	19/09/2017
		Hurricane Irma	06/09/2017

### 3.3 Methods

Figure 6 describes the processes undertaken by the model in order to produce the final erosion, flooding and runoff risk for all the islands in the British Virgin Islands. This was designed as a simplistic risk-based model which could run quickly and be repeatable with minimal data using open-source tools. More complex hydrological models are available which could calculate rainfall-runoff relationships and flow processes more accurately, for example SWAT (Arnold *et al.* 2012) or TopModel (Beven & Freer 2001), however as the BVI had limited data availability for the islands, this method was chosen with minimal requirements, providing an indication of areas under higher risk of flooding during storm events.

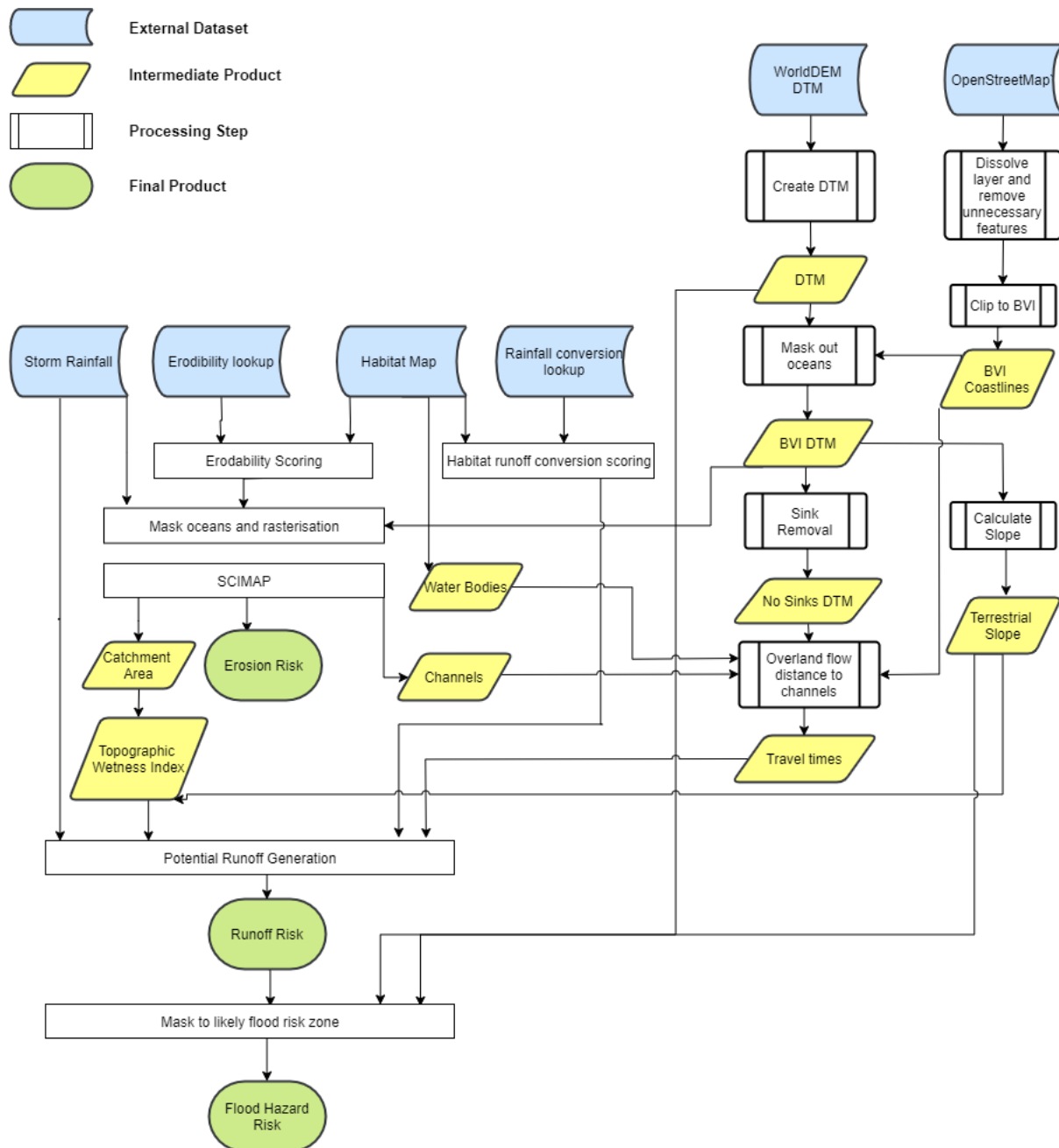


Figure 6: A diagram of the method of the Inland Flooding model.

### 3.3.1 Storm precipitation

The precipitation data for the storm events described in Table 4 were cropped to the extent of the elevation layer, with the maximum value recorded across the BVI applied uniformly to the whole area of interest. Where no records for a storm category were found, the maximum precipitation value was interpolated from a linear model of the maximum values from the examples of other storm categories. For adding into the final runoff risk, precipitation values were scaled on a normalised scale of 0 to 1, with 1 representing a maximum of 150mm of precipitation. This effectively weights the storm risk with storms experiencing higher maximum precipitation levels having larger risk than those in which precipitation levels are much lower.

### 3.3.2 Habitat runoff and erosivity scores

The erosivity and runoff values associated with each habitat class were used to reclassify the habitat map, generating raster layers with the same spatial resolution as the DTM layer. The values are shown below in Table 5.

**Table 5:** Habitat erosivity and runoff values (Perks *et al.* 2017).

No.	Habitat Class	Erosivity Value	Runoff Value	No.	Habitat Class	Erosivity Value	Runoff Value
1	Water	0.01	1.00	11	Scrub	0.10	0.10
2	Sediment	0.01	0.80	12	Rock	0.01	0.00
3	Reef	0.01	0.00	13	Mixed Forest	0.05	0.05
4	Beach	0.01	0.00	14	Urban	0.01	1.00
5	Mangrove	0.05	0.00	15	Bare	1.00	0.80
6	Thicket	0.05	0.10	16	Evergreen Forest	0.05	0.05
7	Salt Pans	1.00	0.00	17	Agriculture	1.00	0.80
8	Drought Deciduous Scrub	0.10	0.10	18	Semi-Deciduous Forest	0.05	0.05
9	Salt Pond	0.01	1.00	19	Seagrass	0.01	0.00
10	Grassland	0.30	0.15				

### 3.3.3 Channel delineation and erosion risk

The SCIMAP (Sensitive Catchment Integrated Modelling and Analysis Platform) Fine Sediment Risk Model developed by Durham and Lancaster Universities, was used to model the catchment network, channels and erosion risk across the landscape (SCIMAP 2017). SCIMAP is a distributed risk-based sediment model using information on land-use and landscape geomorphology to predict the likely movement of sediment and water flows in a catchment (Perks *et al.* 2017).

Figure 7 displays the steps involved in the model, conducted using SAGA version 2.1 64-bit modules and raster calculations (Conrad *et al.* 2015).

The DTM was masked to the island coastlines in order to model just the terrestrial regions. The masked elevation layer along with the habitat erosivity map and maximum precipitation layer derived from the example storm events were aligned and transformed to SAGA grid format by B-Spline Interpolation for use in SCIMAP (Conrad 2007). The SCIMAP model uses SAGA pre-processing modules to first derive the slope from the DTM using the 9 parameters 2nd order polynomial method by Zevenbergen and Thorne (1987). It then removes enclosed depressions in the DTM, which can often interfere with processing steps in hydrological models, by filling these sinks level with the adjacent ground (Williams *et al.* 2017). The catchment/upslope area where flow accumulates is then calculated using a multiple flow direction method and is used along with the elevation to distinguish the channel networks on each of the islands. A multiple flow direction algorithm was chosen for the flow direction calculations as this captured the flow path changes and correlated to the previous outputs produced by Environment Systems Ltd when comparing the channel outputs from the model.

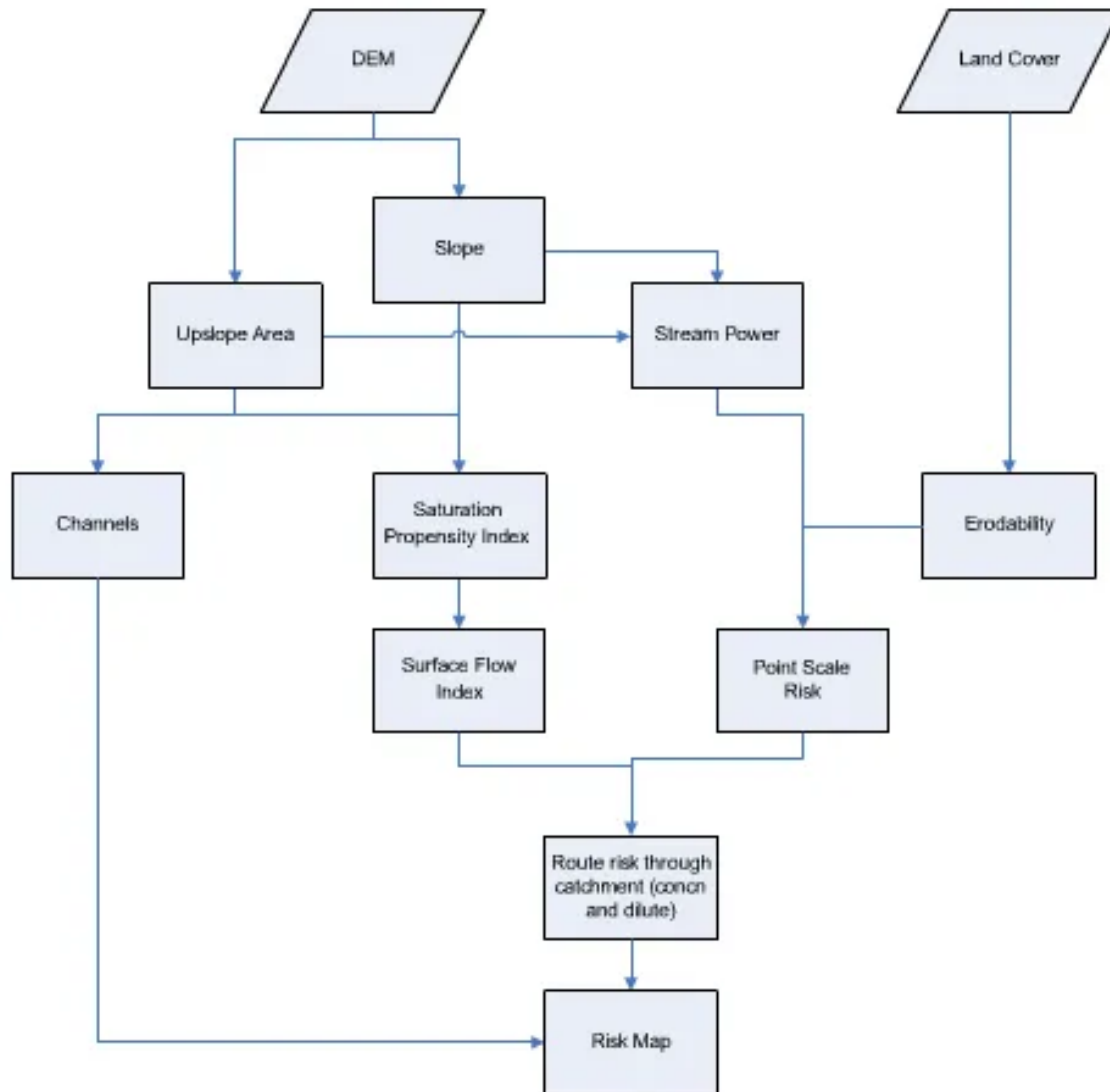


**Figure 7:** A diagram displaying the method conducted by the Fine Sediment Risk Model, incorporating multiple SAGA and raster calculations (SCIMAP 2017).

The SCIMAP fine sediment risk model computes the Topographic Wetness Index (TWI), which is the propensity for each point in the landscape to generate runoff based on topological factors (Reaney 2019, in draft). TWI describes the spatial variation of hydrological processes based upon slope and the upslope contributing area to the flow direction and is often used in hydrologic models as an indicator of the amount of moisture in the soil (Hojati & Mokarram 2016). It is determined through the equation:

$$TWI = \ln \frac{a}{\tan(\beta)}$$

where  $a$  is the specific catchment area and  $\tan(\beta)$  is the slope (Hojati & Mokarram 2016). This is calculated using the SAGA module 'Topographic Wetness Index (TWI)' using the contributing upslope area and a slope layer calculated in radians.

Anthropogenic land modifications are accounted for in the model through supplying a land cover map and a look-up table of relative erodability values. This is used to identify locations where sediment is available for mobilisation and is then compared to the erodability values

to indicate where there is high likelihood of sediment transport within the catchment, using the equation:

$$E = R_w \cdot A \cdot \tan\beta$$

Where  $E$  is erosion potential,  $R_w$  is the assigned risk weighting to each land use class,  $A$  is the upslope contributing area, used as a proxy for the volume of potential surface loss, and the gradient ( $\beta$ ) is used as a proxy for flow speed (Perks *et al.* 2017). Once the catchment erosion potential has been calculated the interaction between sources of sediment erosion and the hydrological connectivity is assessed through a network index, which is calculated by assessing the TWI values required for continuation of downstream flows (Lane *et al.* 2004; Perks *et al.* 2017). The output erosion risk is the rescaled erosion potential, describing where areas of erosion are highest both from the land and within the channels. Although this product was produced in the method undertaken by Williams *et al.* (2017), it was decided not to include it in our analysis. The SCIMAP model assumes that erodability is most influenced by land use and equal across the land use classes regardless of the spatial context and the underlying soil type across the landscape. Therefore, it has limited accuracy in very flat wet landscapes, such as Anegada island in the BVI, as the model is unable to calculate an accurate flow accumulation (Natural England 2015). For this reason, as well as the results being rescaled and so producing modelled outputs which could not be compared across different storm scenarios, these erosion outputs were not included in the workflow and final application.

### 3.3.4 Travel time

As a measure of the magnitude of flood waters remaining in different parts of the catchment, a travel time layer was inferred from calculations of the overland flow distance. This is following the approach taken by the SCIMAP-Flood Model (Reaney & Pearson 2019), whereby a simplified version of a geomorphological unit hydrograph is assessed through calculating flood distances based on terrain analysis. The overland flow distance to the channel network is based on the gridded elevation data, assessing the horizontal and vertical downstream flows to give a true distance measure of each cell to the supplied network based upon the landscape. The gridded elevation was created from the DTM by filling in depressions in the landscape that can cause difficulties in determining flow direction and pathways in hydrological models. There are several algorithms which have been developed for filling in the artificial depressions in DEMs, summarised in Zhu *et al.* (2013). 1D flow direction-based algorithms include Rho4/Rho8 (Fairfield & Leymarie 1991), D8 (O’Callaghan & Mark 1984), D Infinity (Tarboton 1997) and the algorithm developed by Jenson and Domingue (1988) are widely used in GIS software such as GRASS. The previous method by Williams *et al.* (2017) deployed the Jenson & Domingue algorithm through the “r.grass.fill” function in QGIS. In the application presented here, the depression filling algorithm developed by Wang and Liu (2006) called through the SAGA function ‘Fill sinks XXL (Wang & Liu 2006)’ was used, which is designed for working on large datasets. This is often acknowledged as superior algorithm to those previously mentioned as it incorporates spill elevation and least-cost optimal flow paths to simultaneously determine flow paths and watershed partitions (Zhu *et al.* 2013).

The channel network delineated as part of the SCIMAP model was then combined with the coastlines layer and polygons of the waterbodies, which was derived from the habitat map. These together created a shapefile layer of all the outflows where water could flow to either enter the ocean or freshwaters. The overland flow distance was then calculated using the SAGA module ‘Overland Flow Distance to Channel Network’ (Conrad *et al.* 2015) using the multiple flow directions algorithm. The resulting overland flow distance was then normalised

from 0 to 1, with a travel time score of 1 where the distance to an outflow was shortest and a score of 0 representing the greatest distances.

### 3.3.5 Runoff and flooding risk

The Topographic Wetness Index (TWI), habitat runoff scores, travel times and maximum storm precipitation layers were combined by multiplying the relative scores together for each raster cell. These risk values were then categorised into the five risk categories shown in Table 6 based on quantile values from the Category 2 storm example (representative of the range of high and low values).

**Table 6:** The risk categories used to categorise the output layers.

Risk category no.	Risk Scores	Risk Category name
1	0 – 1.53	Very Low
2	1.53 – 1.67	Low
3	1.67 – 1.92	Moderate
4	1.92 – 2.34	High
5	>2.34	Very High

The categorised layer is described as the ‘Runoff Risk’ and is representative of where high levels of runoff are likely to be generated during the storm event. This was then masked to give the likely areas which would be flooded during the event, based on areas as defined by the DTM where slope is less than 30% (Getahun & Gebre 2015) and elevation is below 200m.

## 3.4 Results

The resulting maps described where in the landscape runoff is likely to be generated and areas which are at greater flooding risk from precipitation, where water is likely to pool based upon the landscape terrain, land cover and precipitation.

During a Category 1 storm event, wind speeds are predicted to be between 74-95mph and a maximum precipitation was estimated at 67mm/day. Figure 8 shows the flood risk areas predicted during a Category 1 storm event, with high flooding risk predicted in the low-lying areas around the coast and across Anegada. The predicted runoff generated from a Category 1 storm demonstrates how high surface water flows can develop during storm events, especially from roads across the landscape channelling water into the major towns and cities. High flood risk is predicted around the low-lying major cities of Road Town and Parham Town on Tortola island, with the airport on Beef Island also predicted to have high levels of flooding. 43% of the land area across the Islands is predicted to have some level of risk, 47% of which is predicted at low to moderate flooding risk and 46% of which at high to very high risk. In comparison, the Category 5 storm event example as shown in Figure 9 demonstrates the same pattern of risk in the low lying areas, however the likelihood of risk is far greater with only 9% of at risk areas predicted to be in the low to moderate range and 91% predicted to be in the high risk to very high risk flooding categories. Figure 10 displays how the runoff risk can also dramatically change with a Category 5 storm event where greater precipitation levels are expected and high runoff is predicted particularly in low lying areas.

The flood risk is generated through masking the runoff risk to predicted flooding zones, derived by thresholding the slope and elevation with threshold values established through literature reviews. This limits the model’s prediction of flood risk areas and delineates only

the areas of expected standing water, as opposed to representing both the surface water runoff and standing waters experienced during a flood event. This is due to the simplicity of the models providing a snapshot estimate of where flooding is likely to be a risk using minimal data inputs, and as the method is not a distributed hydrological model it is unable to quantify water depth of standing water and flows. As the models use an estimate of the maximum precipitation experienced during the storm event, they are unable to monitor how flood risk will vary as the storm progresses or consider storm duration and the impact of the soil saturation levels prior to an event taking place.

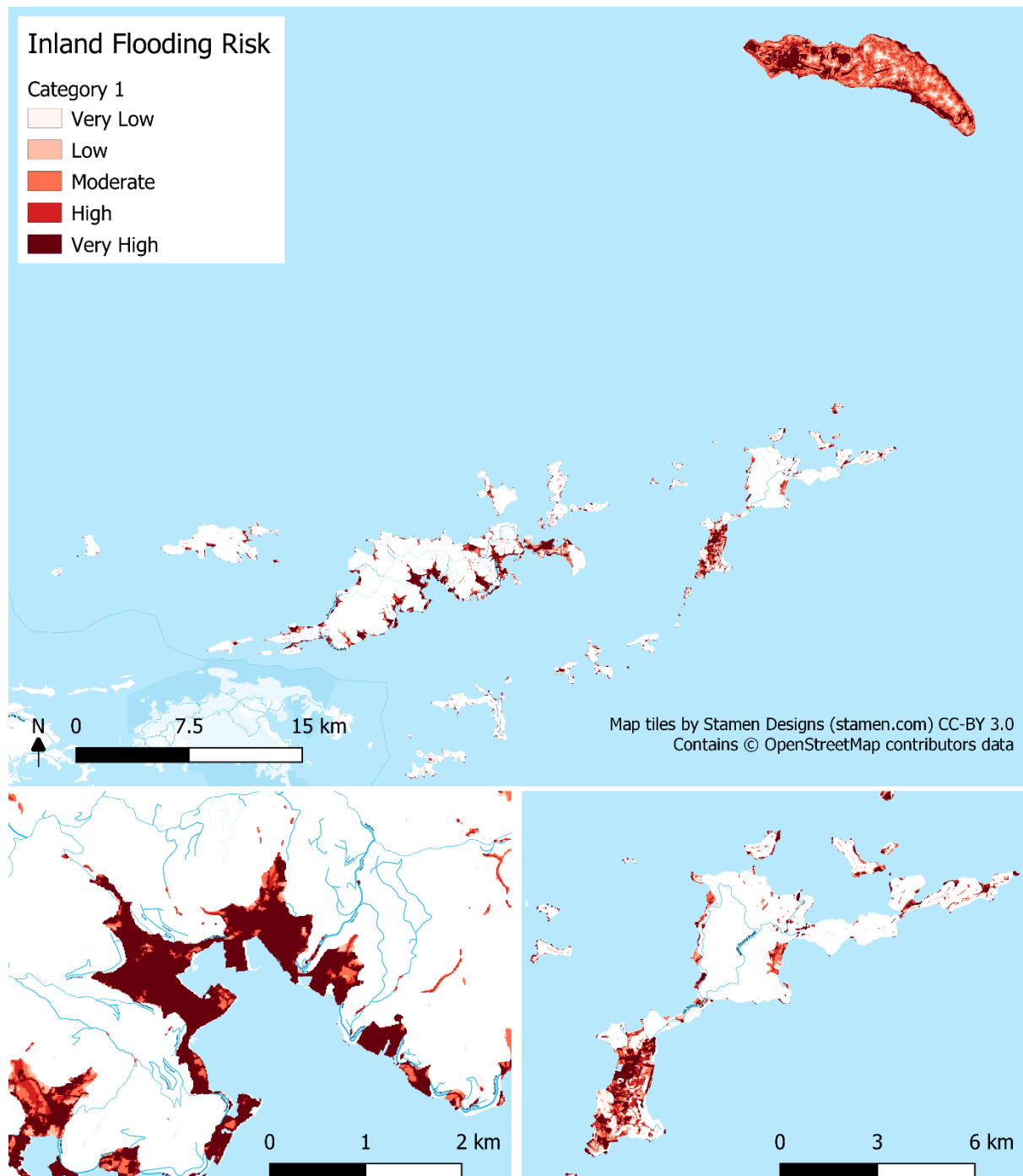


**Figure 8:** Predicted Flood Risk during a Category 1 Storm Event; (top) the whole of the British Virgin Islands, (middle) Road Town, Tortola, and (bottom) Virgin Gorda islands.

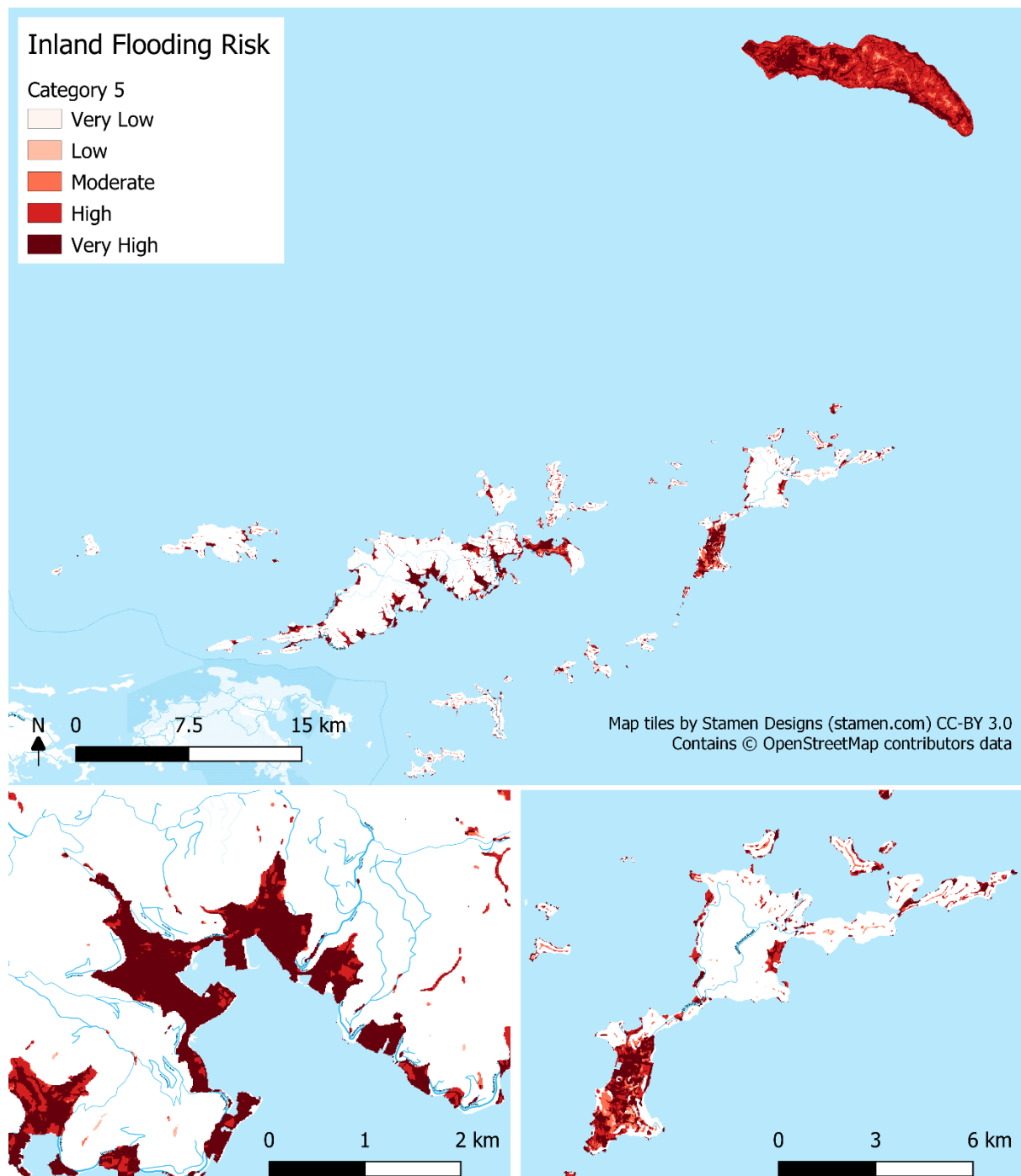


**Figure 9:** Predicted Flood Risk during a Category 5 Storm Event; (top) the whole of the British Virgin Islands, (middle) Road Town, Tortola, and (bottom) Virgin Gorda islands.

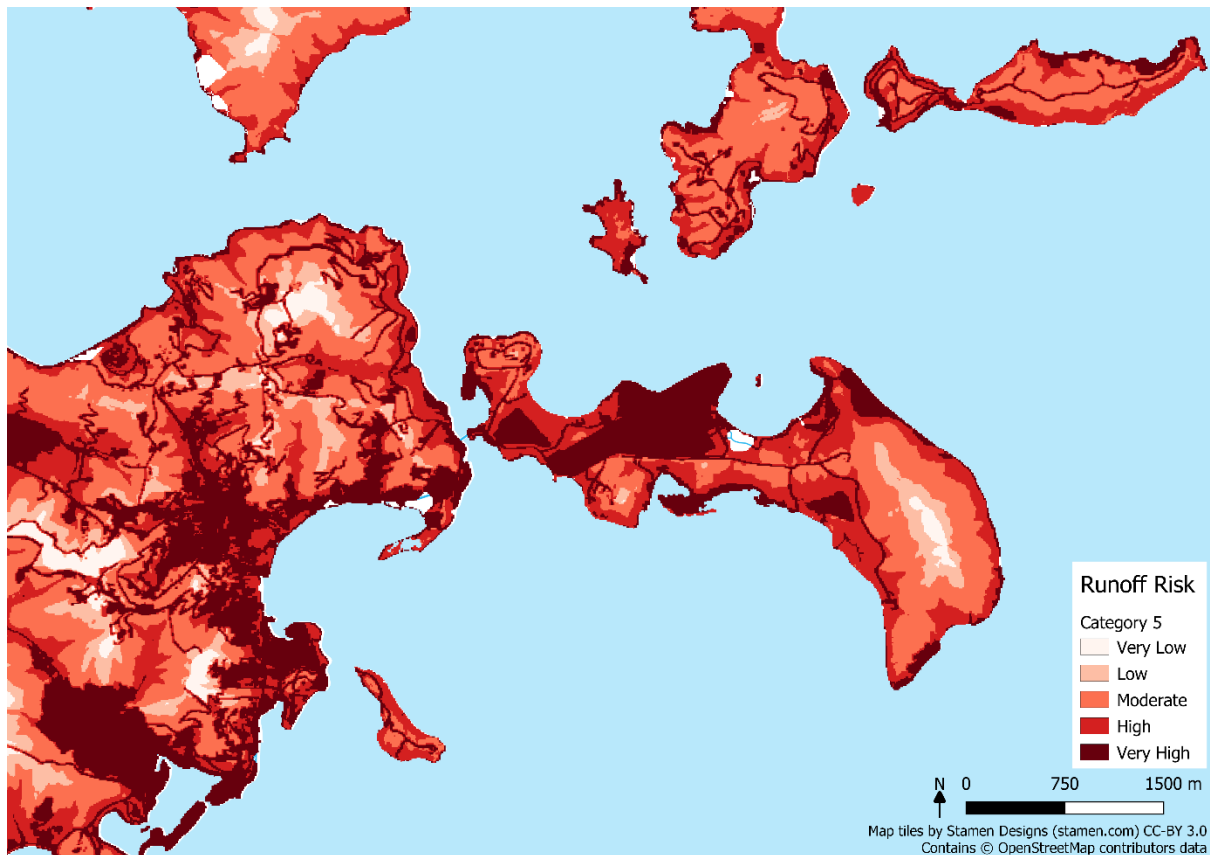


**Figure 10:** The Runoff Risk modelled for a Category 5 Storm Event, showing Beef island on the northern tip of Tortola, BVI.

Two examples reported to have had devastating impacts upon the Islands were Hurricane Irma which struck on 6 September 2017 and Hurricane Maria which hit just 13 days later, on 19 September (NOAA NHC 2020c). Both were classed as Category 5 storms however Maria was a much wetter event, with a maximum precipitation approximated here as 119 mm/day as opposed to Irma which experienced a maximum precipitation of 68mm/day. The difference in storm characteristics is evident from the predictions shown in Figure 11, where the predicted runoff is vastly greater across the islands during Hurricane Maria than Hurricane Irma. Hurricane Maria took place just 13 days after Irma, so it is expected the ground was already saturated leading to increases in flood damage. This model was unable to consider the oversaturation and degraded conditions of the habitats, and so the risk would be expected to have been even greater than that predicted below.

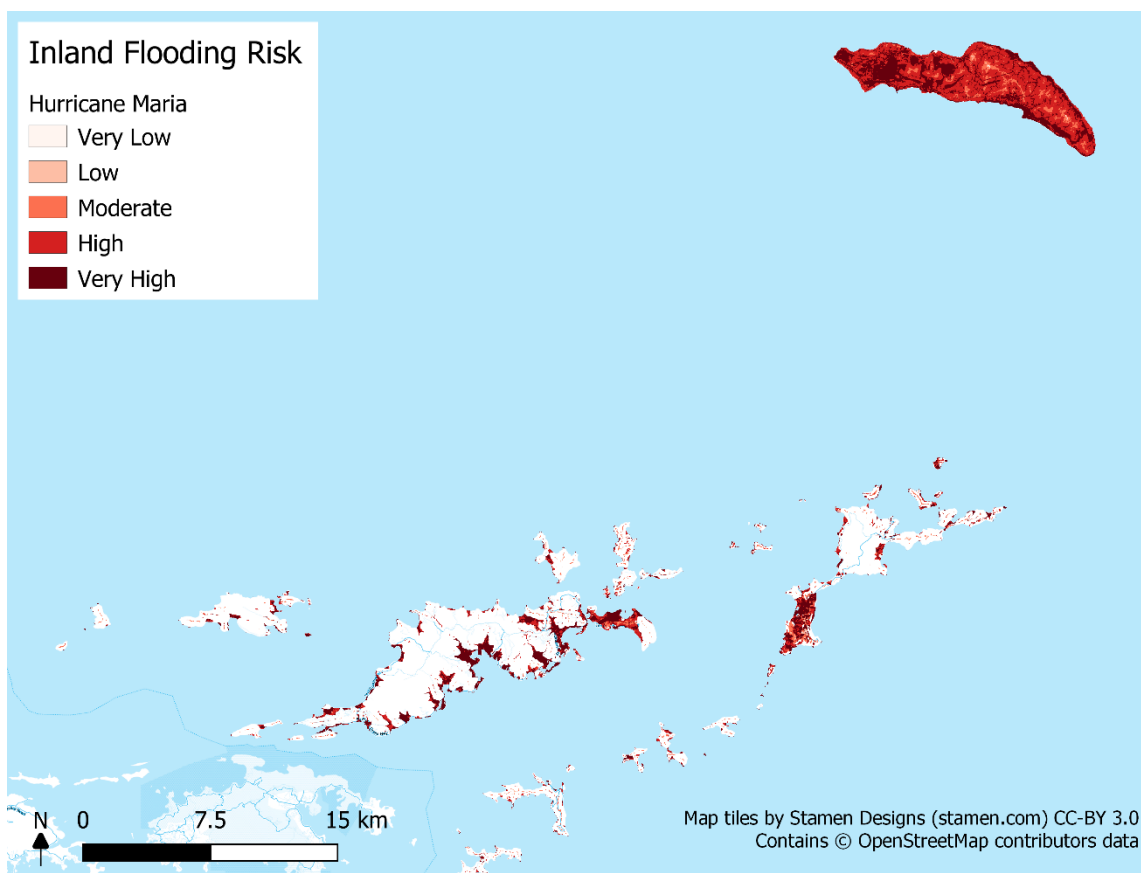
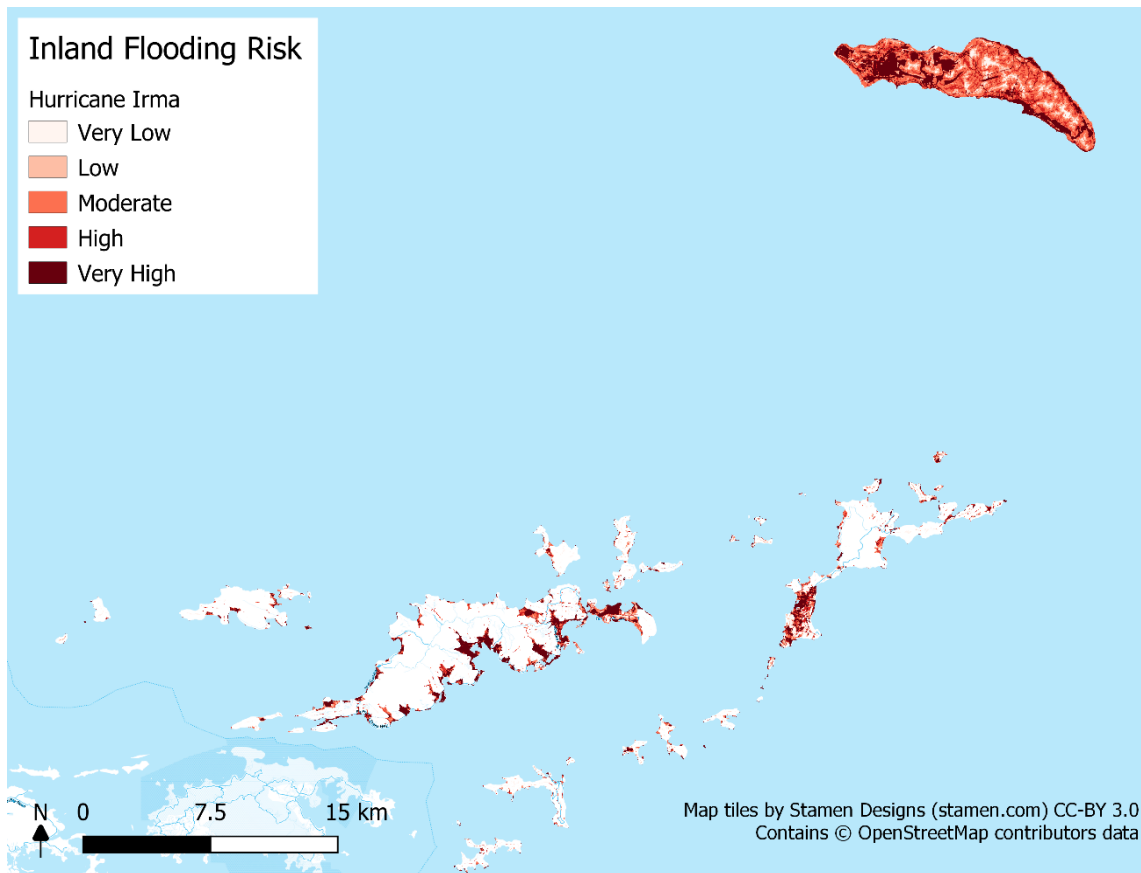


**Figure 11:** Predicted Flood Risk during the Hurricane Irma (top) and Maria (bottom) storm events during the 2017 hurricane season.

## 4 Combined Risk

The outputs from both the Storm Surge Terrestrial Risk and Inland Flooding Risk models were combined to generate one overall risk map of terrestrial flooding, shown in Figure 12. This was calculated by taking the highest risk category for a given cell from the two input layers, the highest value being chosen as this minimises underprediction of risk. As a conservative approach, where both layers predicted the same level of risk, for example moderate risk of inland flooding and moderate risk of storm surge, these were reclassified into a higher risk category, taking into account the cumulative impacts of both model predictions.

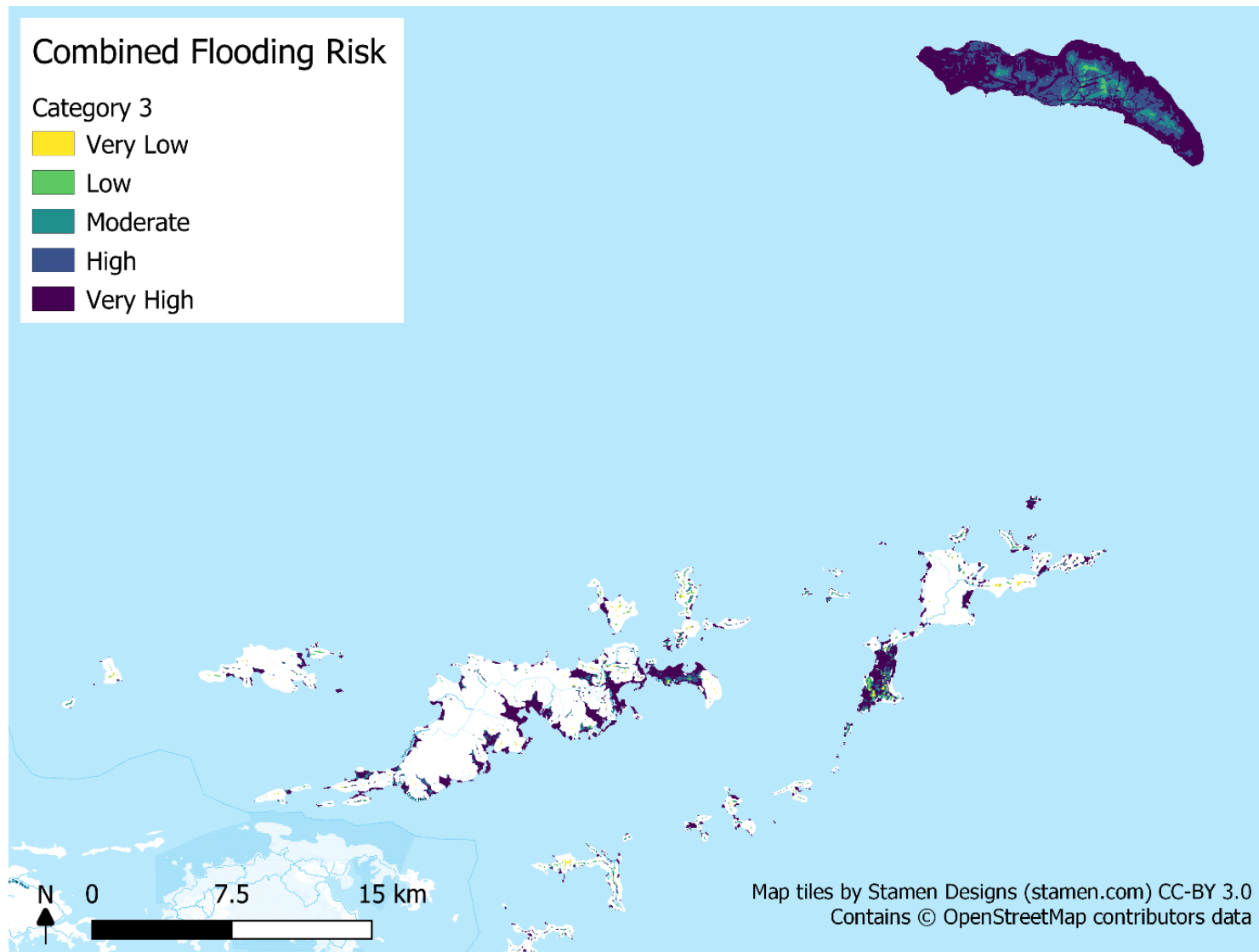


**Figure 12:** Combined Flooding Risk for a Category 3 Storm Event.

## 5 Model Validation

The models were validated by comparing model predictions with the outputs of storm surge and inland flood risk modelling which has been carried out previously in the BVI under JNCC contracts with Environment Systems Ltd (Williams *et al.* 2018) and Wood PLC (Bray *et al.* 2019), to assess how well predictions of risk align between the different modelling approaches.

### 5.1 Storm surge model validation

Williams *et al.* (2018) as part of the vulnerability assessment of the BVI conducted after the 2017 hurricane season, delineated damage from the storm surge produced by Hurricanes Irma and Maria, which was reported to be approximately 6.2 metres high. This was a visual interpretation developed from Worldview-2 and Pleiades data. As well as satellite imagery, social media was also used to confirm the damage lines. The damage layer is split into 'visual' where actual damage was clearly visible from the imagery, and 'potential' where water or storm surge damage was likely but obscured in the imagery by vegetation. These were focussing on the damage in the aftermath of Hurricanes Irma and Maria, however further validation could be carried out with other storm events, particularly of lower categories on the Saffir-Simpson scale, in order to validate model predictions under storms of lower windspeeds.

From visual assessments against the damage line it is evident that the modelled predictions for the Hurricane Irma storm example closely aligned with the areas where flood damage was observed, as shown in Figures 13 and 14. The storm surge model generally overpredicts in the low-lying regions, with over 50% of the area outside of the damage lines on Beef Island predicted as Moderate to Very High risk. On Anegada, 94% of the island outside of the damage lines was predicted between Moderate to Very High risk, with 86% in the High to Very High risk categories. However, the damage line assessment was carried out with satellite imagery several days after the event due to needing cloud free images, therefore the actual damage may have been more widespread than that indicated.

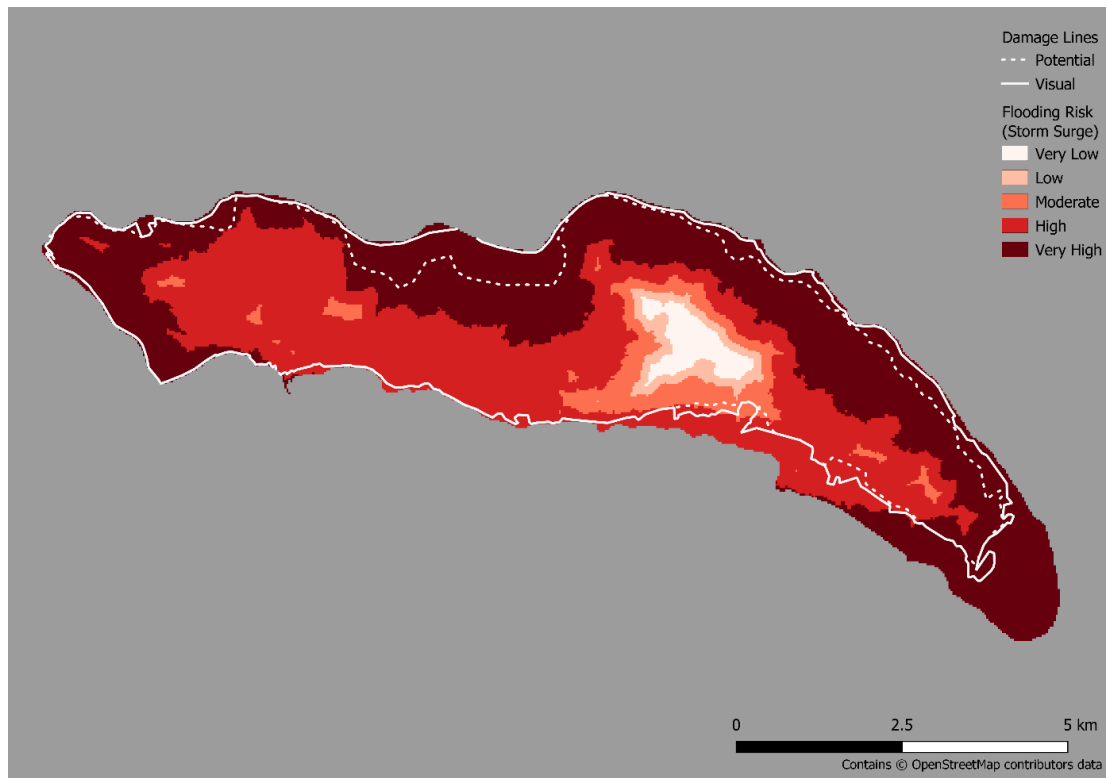


**Figure 13:** Comparisons of the damage line derived from visual assessments of the aftermath of Hurricanes Irma and Maria (Williams *et al.* 2017), against the modelled prediction of risk from the Hurricane Irma storm surge model example for Anegada.

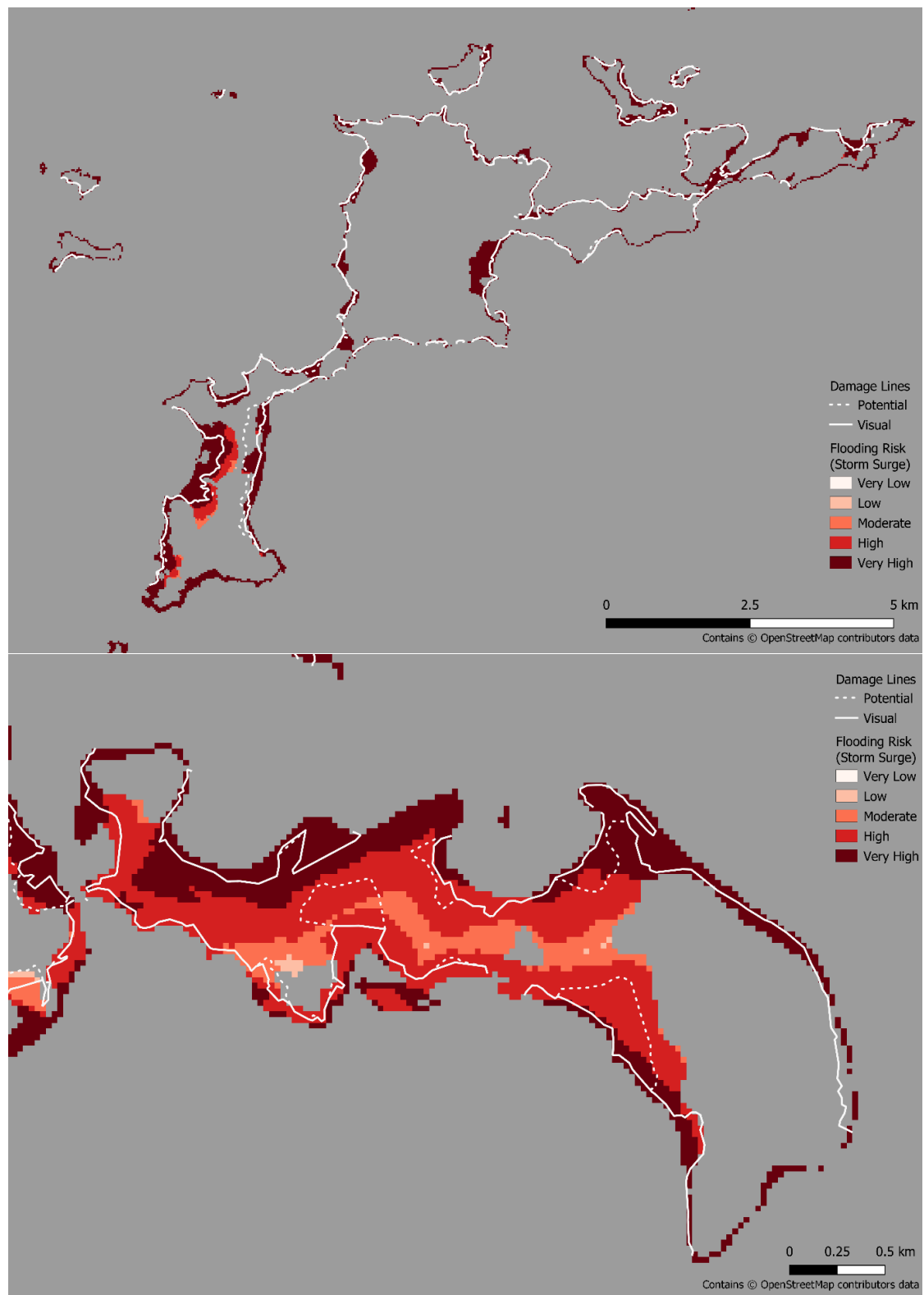


**Figure 14:** Comparisons of the damage line derived from visual assessments of the aftermath of Hurricanes Irma and Maria (Williams *et al.* 2017), against the modelled prediction of risk from the Hurricane Irma storm surge model example. The maps show close-ups of Virgin Gorda (top) and Beef Island (bottom).

This close alignment was evident from assessing the modelled results from within the polygonised damage line regions, which was conducted as part of the sensitivity analysis for the storm surge risk model. For Anegada, all the area where visual or potential damage was

observed was predicted as being under moderate to very high risk by the storm surge model. Of this, 97% of the visual damage was predicted to be in the highest two risk categories of inundation from storm surge. The damage on Beef island, where importantly the airport is located, showed similar accuracy with 91% of the visual damage and 98% of the potential damage predicted as moderate to very high risk. Finally, the Virgin Gorda island group predictions had a high accuracy for the visible damage, with 95% predicted in our models as being under moderate to very high risk. For the potential damage line this fell to 67% predicted in these risk categories. However, this is likely due to the nature of the model establishing the likely coastal flooding area to be under 20m, with some of the potential damage being noted in areas over 20m elevation. The underprediction in regions could also be due to the damage lines being created after both Irma and Maria, with the outputs from the Irma storm alone being used here for comparison. During Hurricane Maria the islands experienced much greater precipitation levels, which when falling on already saturated land could cause damage from flooding that would have exceeded our modelled predictions from just Hurricane Irma. Additionally, observed damage would likely have been a combination of many factors, including wave action, flooding from precipitation, and wind damage, and not just damage from storm surge, the risk of which is modelled here.

## 5.2 Inland flood model validation

Bray *et al.* (2019) conducted several case studies of major cities and towns in the BVI, modelling inland flooding risk using a 2D hydraulic model developed in InfoWorks ICM (Integrated Catchment Model). The modelled outputs of their scenario reflecting conditions for a storm event occurring 1 in 100-year annual exceedance probability, simulating an intensive rainfall event during a hurricane, was compared to the results of the inland flooding model for the example parameters simulating Hurricane Maria. During Hurricane Maria there was significant rainfall as it passed through the region estimated to cause US\$3.6 billion in damages (UNDP 2017).

Comparing the outputs from Bray *et al.* (2019), the model highlights similar regions along the flow path where flooding is likely to occur during an extreme rainfall event. Bray *et al.*'s case studies were at varying resolutions, with hydrological meshes created at 5-15m and 25-50m spatial resolutions modelling detailed scenarios at sites of interest. This was compared to the inland flooding outputs for Hurricane Maria produced by the model described in Section 3, modelled at 10m spatial resolution. Therefore, differences in the scale of the data may explain some of the difference between the predictions. The outputs also differed in their risk scales, where the Flood Hazard rating for Bray *et al.* (2019) were categorised as 'very low hazard', 'danger for some', 'danger for most' and 'danger for all'. These were translated to the categories used in our analysis as 'Very Low', 'Moderate', 'High' and 'Very High' respectively.

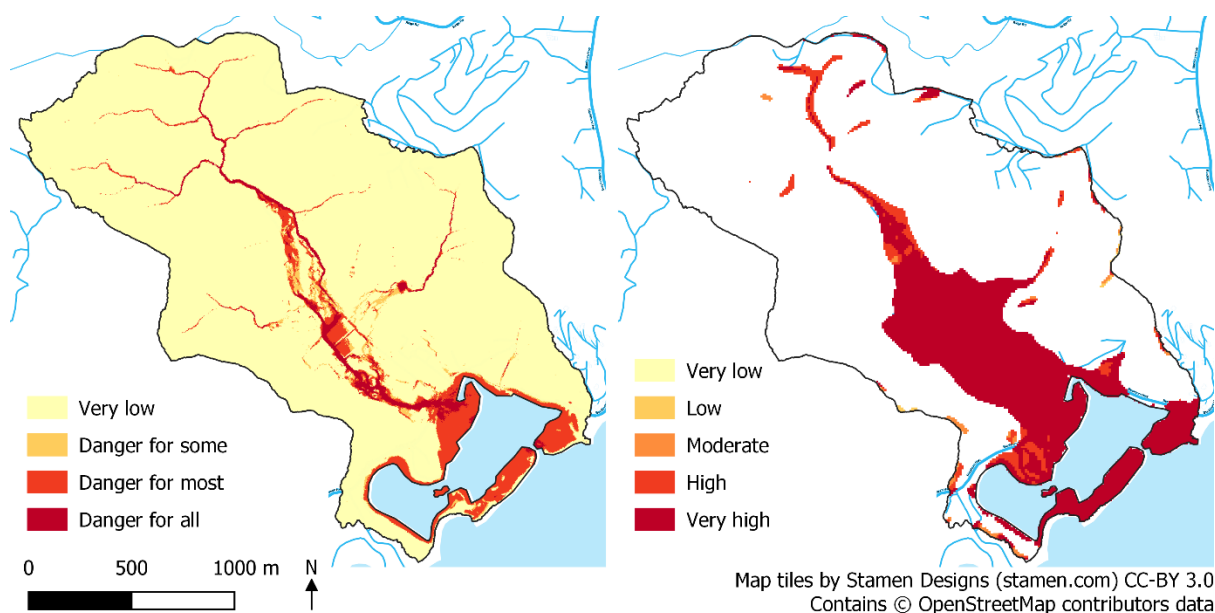


**Figure 15:** Comparison of the Wood detailed modelled outputs (left) with the coarser predictions from the Inland Flooding Model (right) for Paraquita Bay.

Comparing the two modelling approaches, our model generally overpredicted areas at risk in comparison to Bray *et al.*'s modelled outcomes, with on average 12.94% more of the modelled area being predicted at moderate to very high risk. Of the areas that their analysis predicted as moderate to very high risk, on average 82.35% were also predicted in the same risk bands by our model, the majority of which fell under the 'Very High' category. This varied depending on the case study, with 68.29% of areas in Cane Garden Bay but 95.29% of areas in Beef Island falling within the same risk categories. When these were further subset to just those predictions in the high and very high category, the mean percentage correctly predicted Moderate to Very High by our models was 82.04%. This showed similarity between the modelled outputs, despite the obvious differences in resolution and the complexities of the models. Despite being a relatively simplistic model, the predictions from our inland flooding model were able to derive the areas at high risk of flooding to people with good accuracy when compared to results from a 2D hydrological model created with specialist software.

## 6 Risk Modelling Application

To make the models more accessible to stakeholders, an R Shiny application was developed using "shinydashboard" (Chang *et al.* 2018). The application incorporates both the Inland Flooding and Storm Surge models allowing non-technical users to not only view the results of the models with example storm conditions, but to run through them themselves with different storm paths and storm conditions, and to assess the effect that changes in land use have on modelled risk. This user-friendly application allows users to explore the output risk maps interactively, zooming in on areas of interest and downloading the results.

The app consists of five tabs, shown in the screenshots in Figures 16 to Figure 17.

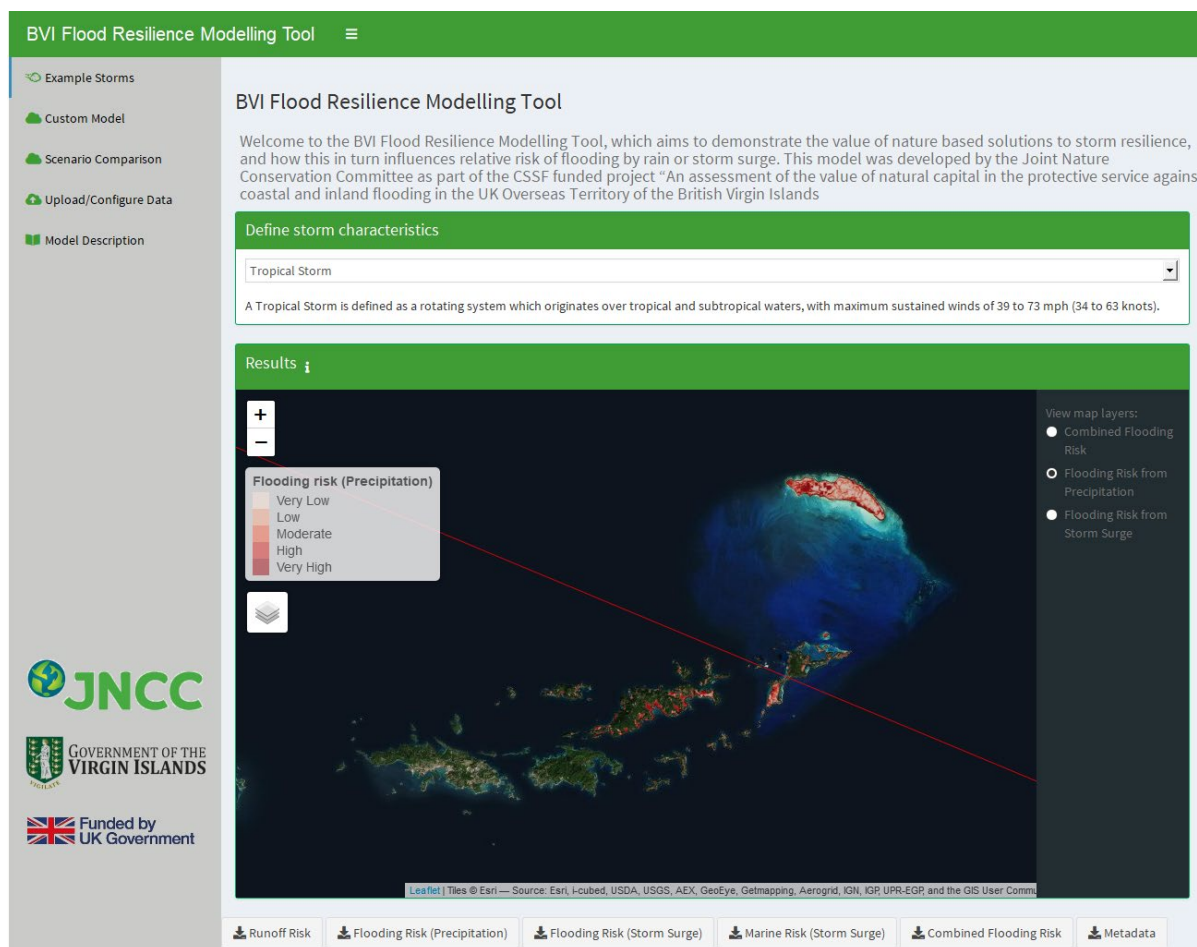


Figure 16: Landing page, with modelled outputs from pre-run examples.

The landing page displays maps from example storms along with a short description of the specified storm category. A dropdown menu allows the user to select from the modelled examples of a tropical storm and Category 1-5 hurricanes, all run with the same path at 30m spatial resolution. Two additional examples of Category 5 hurricanes, Hurricanes Irma and Maria, were also included as these dramatically impacted the islands, with very differing effects despite both being classed as Category 5. The user can download the individual risk maps as raster files along with a metadata document, so further analysis can be conducted with the outputs. The interactive map display lets them zoom in and out, turn on and off layers and change the layer transparency.

The second tab allows the user to run the models themselves with customised storm parameters. The user can draw or upload a storm path passing through the given area of interest around the islands, and then specify their storm conditions by inputting a custom precipitation value and selecting the storm category from the dropdown menu. They can then select which output layers they wish to view, thus choosing which models to run before clicking on the 'Submit' button. This will rerun the sections of the models which are affected by the new inputs, using archived data layers where possible to decrease processing time. Whilst these run, the user will be updated with messages describing what stage in the modelling the application has reached. Once finished, the Results tab will be populated with the selected risk outputs displayed in interactive maps and they can again download the results as raster files.

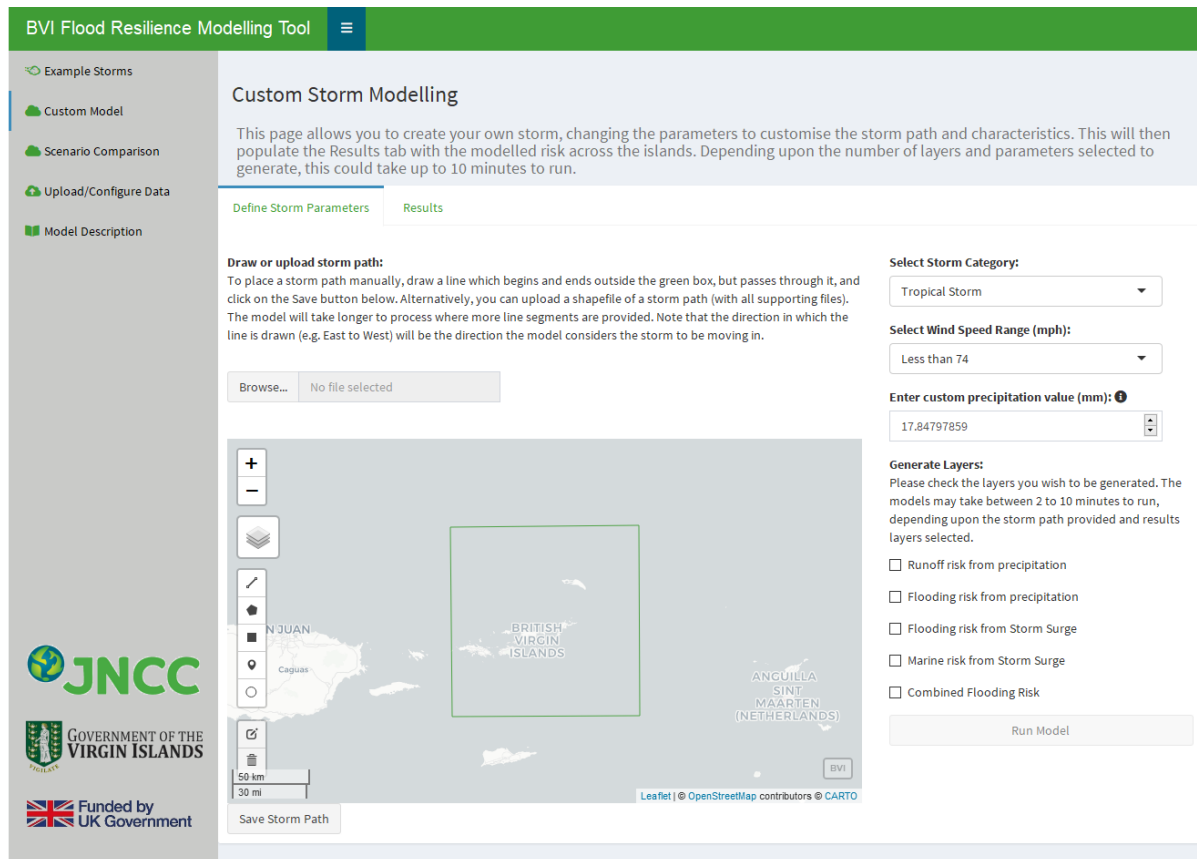
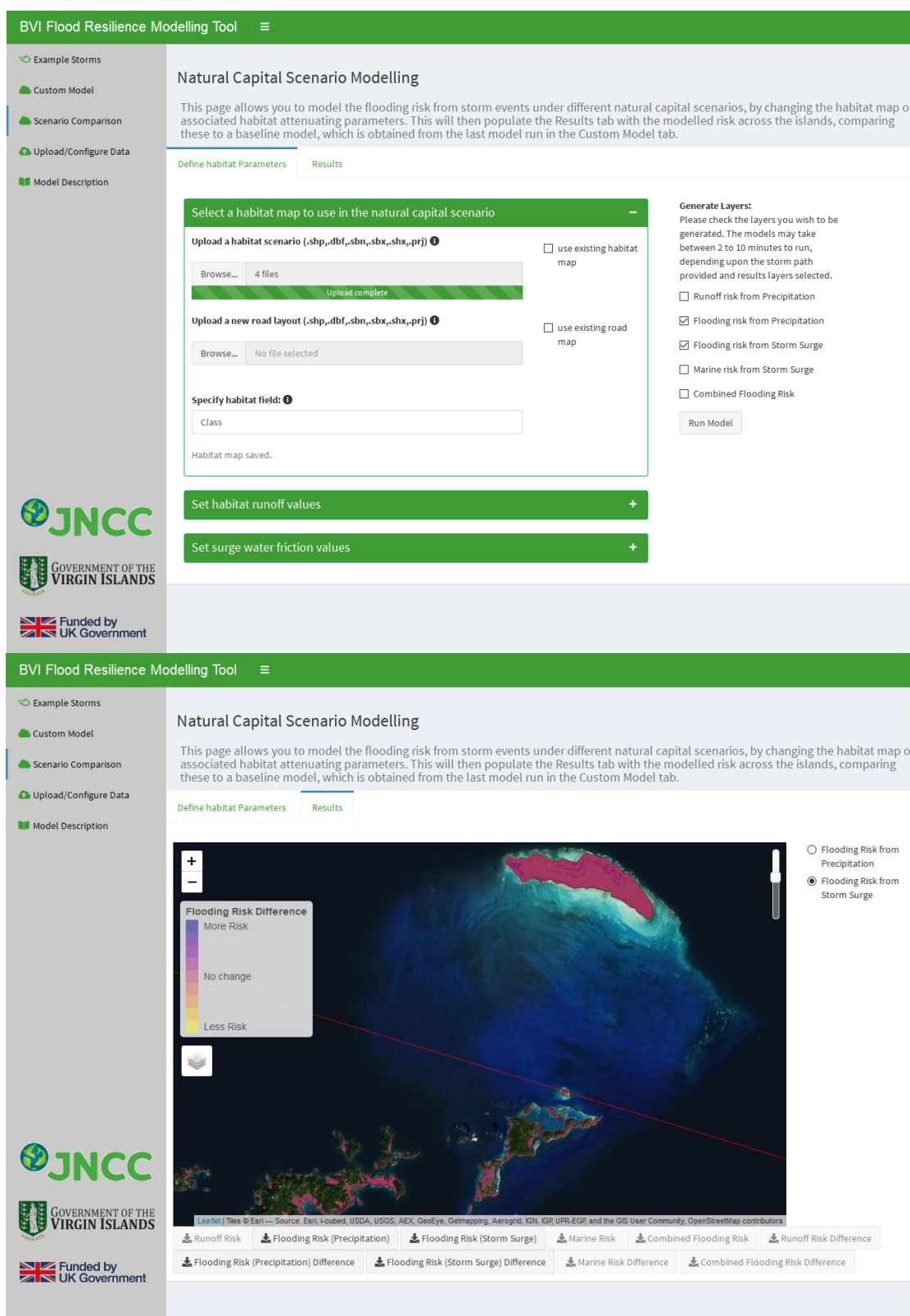


Figure 17: Screenshot of the 'Custom Storm' tab where users can model their own storm parameters.

The third tab titled "Scenario Comparison" lets the user utilise the models for assessing different natural capital scenarios on the islands. The user can upload a new habitat map, road layer or update the friction and runoff conversion values associated with each habitat class to alter their impact on flooding risk. The models are then rerun under the changed habitat conditions, and the results are compared to those of the previous model run in the "Custom Model" tab. The "Results" tab displays the relative flood risk from precipitation and storm surge both before and after the change implemented in the scenario, as well as the difference between the two layers, so that the user can interrogate how their risk categories are changing. These are shown in Figure 18.



**Figure 18:** The scenario comparison tab in the application, showing the results for Flooding from Storm Surge under a scenario where the mangroves were removed. Toggle between A) setting the parameters of the scenario, and b) displaying comparison outputs [or similar]

The fourth tab (Figure 19, top) lets the user edit the underlying archived layers used in the custom model; by supplying new elevation, bathymetry, habitat and roads layers, editing the runoff conversion and Manning’s n values associated with habitat classes, and changing the

output spatial resolution. Any functions in the two models which are impacted by the changes to layers are rerun, again to save computational time. The “Reset” button also allow the user to reset these layers to the previous archived versions which were used to run the examples. The final tab (Figure 19, bottom) provides a description of the project, the method implemented in both models, and their limitations.

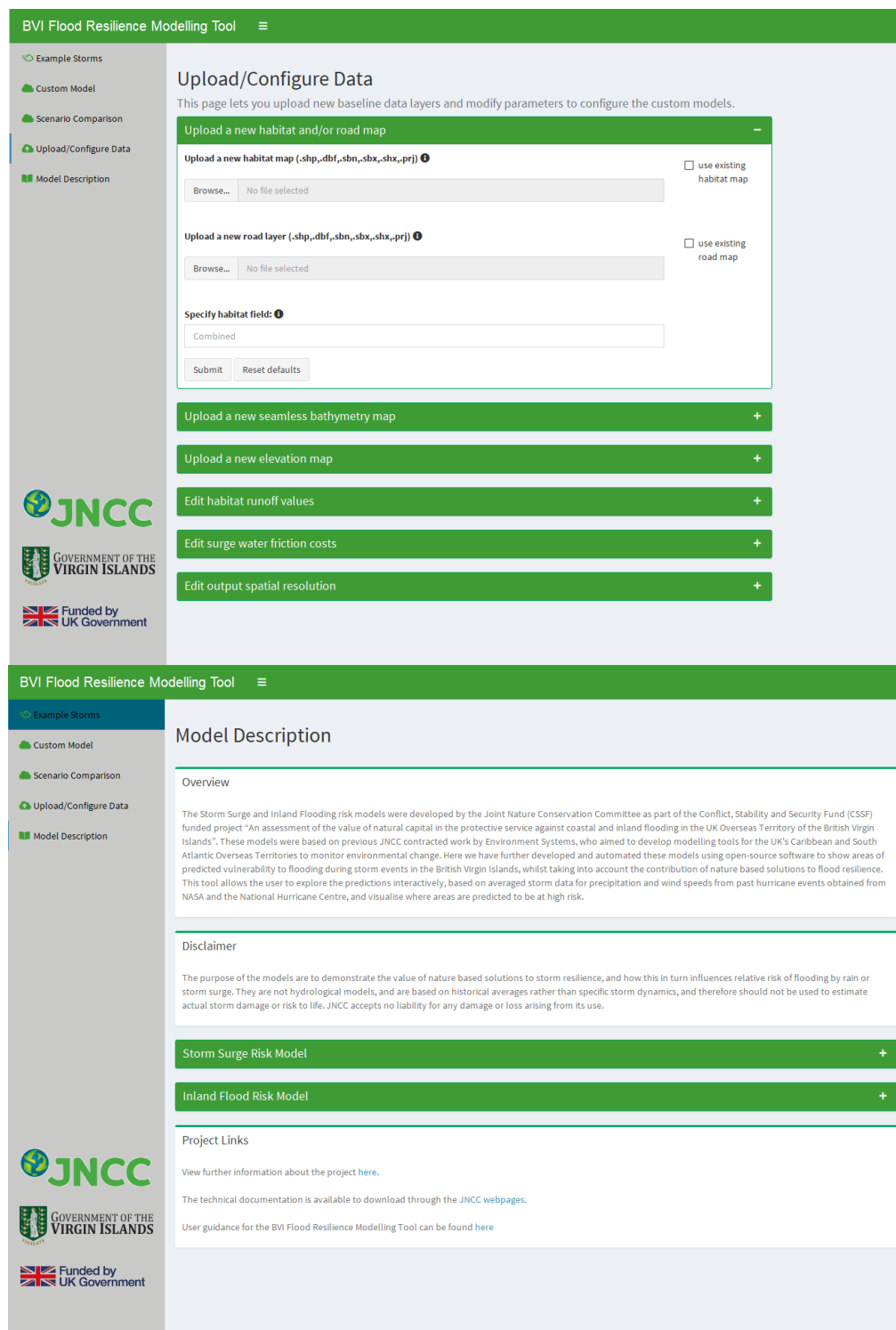


**Figure 19:** Screenshots of the tab pages “Upload/Configure Data” (top) where users can change their baseline input layers the models are run with, and the “Model Description” (bottom) tab which provides more information on the models and their limitations.

## 7 Natural Capital Assessment

To assess the value of natural capital and its protective capacity to reduce coastal and inland flooding, the models were applied to various scenarios to see how predicted risk varied with changes to natural capital assets. Through the workshops it was identified that increasing numbers of roads were a key concern for inland flooding, with urban expansion causing greater numbers of roads to be created, impacting the drainage rates by channelling runoff and increase pooling in the low flat regions of the islands. With regards to reducing the damage from storm surge, mangroves are often cited as a nature-based solution to absorb the energy of a surge before it makes landfall, helping reduce the wave height by between 13% and 66% for over 100m of mangroves or by between 50% and 99% for over 500m of mangroves (Bray *et al.* 2019; Spalding *et al.* 2014; Dasgupta *et al.* 2019). To explore these ideas further, the habitat map was edited to simulate various scenarios with each of the models:

- Storm Surge:
  1. Remove all the mangroves
  2. Increase the width of the mangroves
  3. Degrade the mangroves
- Inland Flooding:
  4. Remove all the roads
  5. Remove roads at elevations over 100m
  6. Expand urban areas

The models were rerun using these new habitat maps under Category 3 storm conditions, and then assessed against a baseline example for a Category 3 storm.

### 7.1 Storm surge scenarios

#### 7.1.1 Remove all the mangroves

To explore the protective service provided by the mangroves, a scenario where the mangrove habitats were removed was remodelled with an example Category 3 storm. The habitat map was updated with these habitats converted to “bare ground” and the predicted risk was compared to the baseline scenario. In most cases, although terrestrial risk was altered there was not a great enough level of change to result in a risk category change, with risk categories decreasing in 0.4% of areas and increasing in 19.8% of areas. An interesting example of the effect can be seen in Paraquita Bay (Figure 20, left), where mangroves are currently used directly for their protective service (sheltering yachts in storm conditions), and where the removal of mangroves clearly increases risk in currently mangrove-sheltered areas.

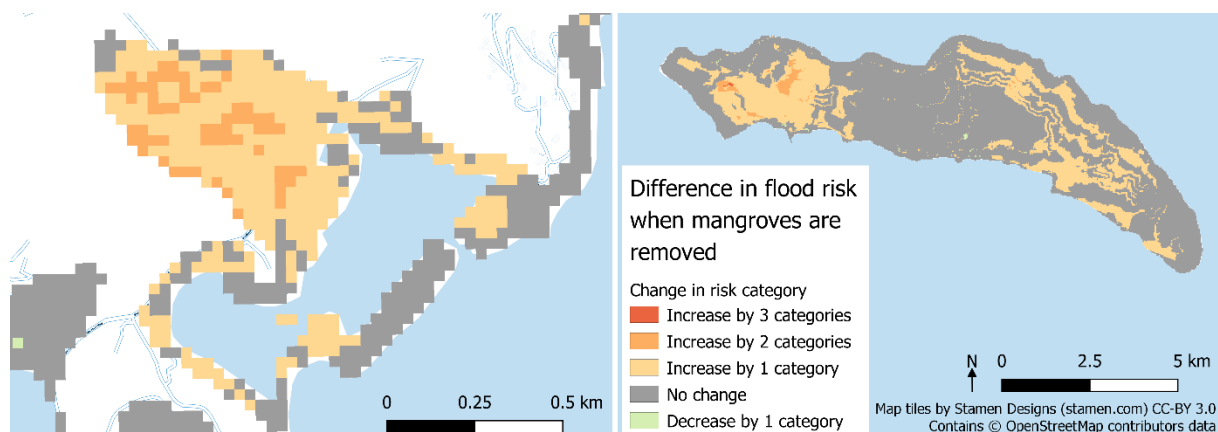


**Figure 20:** Change in predicted terrestrial flooding risk from storm surge when mangrove habitats are removed, compared to the baseline scenario. This simulation was run with the example ESE storm track as a Category 3 storm. Modelled risk increases in areas such as Paraquita Bay (left) and Anegada (right).

The linear increases in risk observed on Anegada are likely to be a result of the quantiling process: as areas of higher risk expand, their boundaries are pushed from one risk category into the next, therefore giving the effect of risk changing in bands seen here.

### 7.1.2 Buffer the mangroves

A scenario where the mangrove habitats were expanded was modelled by buffering mangrove habitats by 10m. When modelled as a Category 3 storm, 0.7% of areas see increasing risk and 5.0% of areas see decreasing risk (Figure 21). The results for Anegada under the scenario demonstrate how the buffered mangrove habitats around the island help to increase the storm attenuation service being delivered and thus displaying a decrease in the expected risk category across the island.

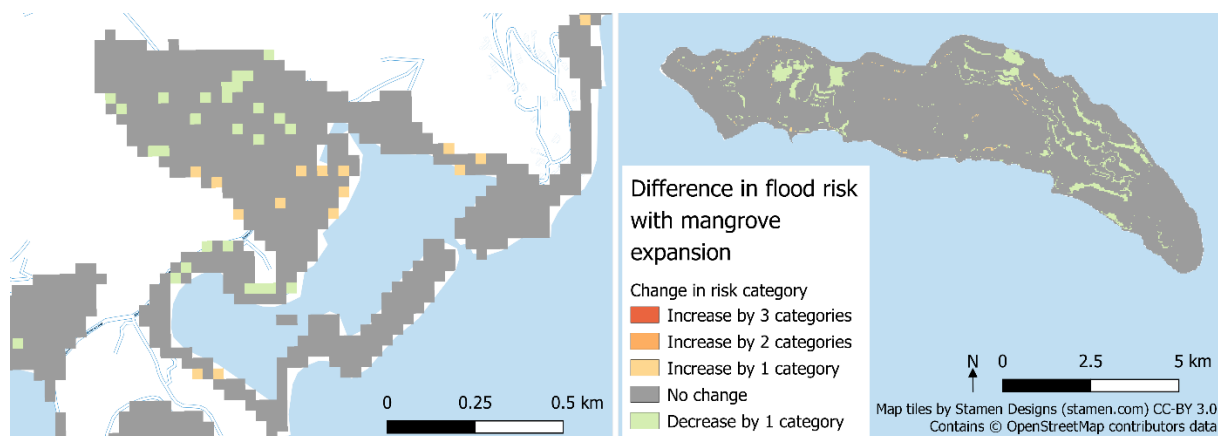


**Figure 21:** Change in predicted terrestrial flooding risk from storm surge when mangrove habitats are expanded, compared to the baseline scenario. This simulation was run with the example ESE storm track as a Category 3 storm. Example outputs are presented for Paraquita Bay (left) and Anegada (right).

### 7.1.3 Degrade the mangroves

A scenario where the mangroves were degraded was run by halving the Manning's n coefficient for mangrove habitats from 0.1 to 0.05, simulating the reduction in friction the mangroves provide and their ability to attenuate surge (Figure 22). The scenario demonstrated increases in risk in 4.4% of areas, and decreased risk in 5.3% of areas. As

observed in the removed mangrove scenario, areas such as Paraquita Bay currently known for their protective service are seen to increase in risk.

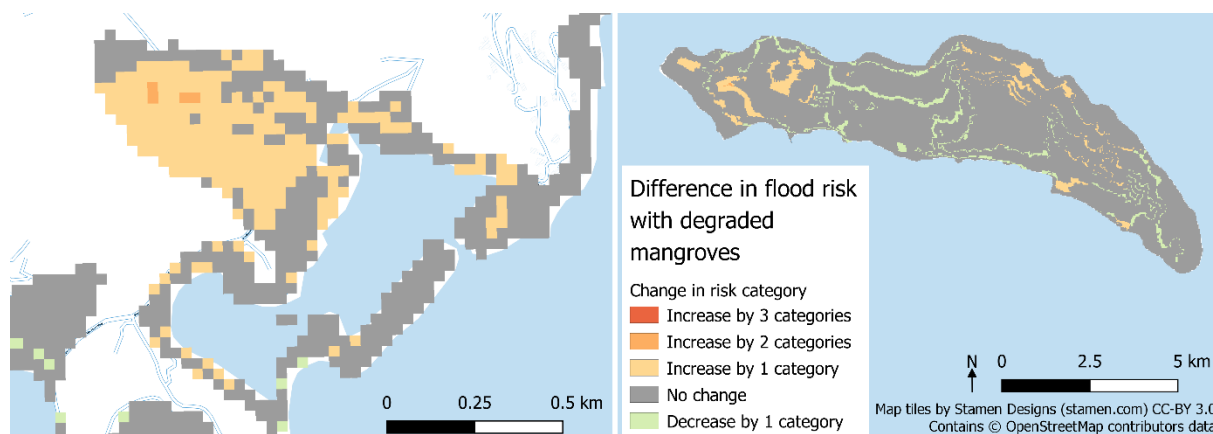


**Figure 22:** Change in predicted terrestrial flooding risk from storm surge when mangrove habitats are degraded, compared to the baseline scenario. This simulation was run with the example ESE storm track as a Category 3 storm. Example outputs are presented for Paraquita Bay (left) and Anegada (right).

Interestingly here we also observe decreased risk in some areas, an effect also seen to a much lesser extent in the other storm surge scenarios, contrary to the change expected. At present it is unclear why we see this, and this requires further investigation.

## 7.2 Inland flooding scenarios

### 7.2.1 Convert all roads to grassland

To explore the impact roads are having on the predicted runoff and flooding risk in the inland flood model, the roads were converted to grassland, simulating a scenario where these were all removed. The results shown in Figure 23 demonstrate the impact roads are predicted to have on the damage risk from runoff.

Risk overall is reduced, with this effect being most prominent inland at the higher elevations, reducing the risk by up to 4 categories in the areas at high relief, from being classed as 'Very High' to 'Low' risk. In the lowland areas where risk is already high due to impervious surfaces from urban areas and being at lower elevations where water is more likely to pool from overland flow, risk is only reduced slightly in comparison. This analysis shows that the addition of the roads at higher elevations may have substantially increased the risk of damage from runoff during extreme rainfall events. *Sixty percent (60%)* of the area which changed risk category experienced a reduction by 1 risk category, whereas 8% experienced a reduction of 3 or 4 categories. This scenario assumes conversion to grassland, however previous land use cover prior to the roads being built may have differed where runoff conversion values may have been better or worse than that of grassland.

### 7.2.2 Convert roads at elevations over 100m to grassland

This scenario again shows similar conclusions to the previous scenarios where roads were converted to grassland, although highlights how even small changes such as the removal of hilltop roads at elevations over 100m can have a relatively large reduction in the potential for runoff generation. The roads were again converted to grassland, which has reduced the runoff risk for these areas shown in Figure 24. Fifty percent (50%) of the changes in risk category were a decrease in one category, whereas 17% of the changes noted were a reduction in three or four risk categories. This would suggest in some areas above 100m

that reducing the roads and converting these to grassland would greatly help to alleviate high levels of runoff during storm events.

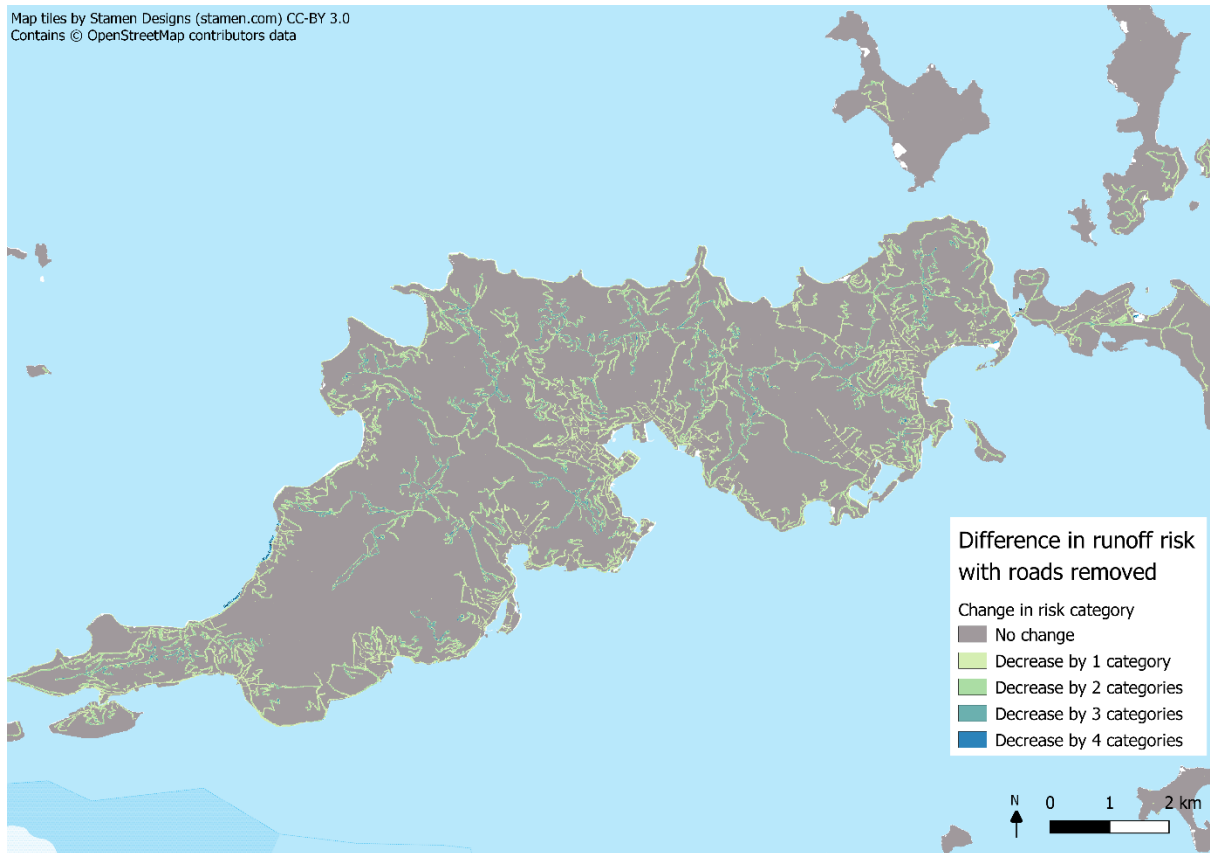


**Figure 23:** Modelled difference under natural capital scenario 1 where all roads were removed.

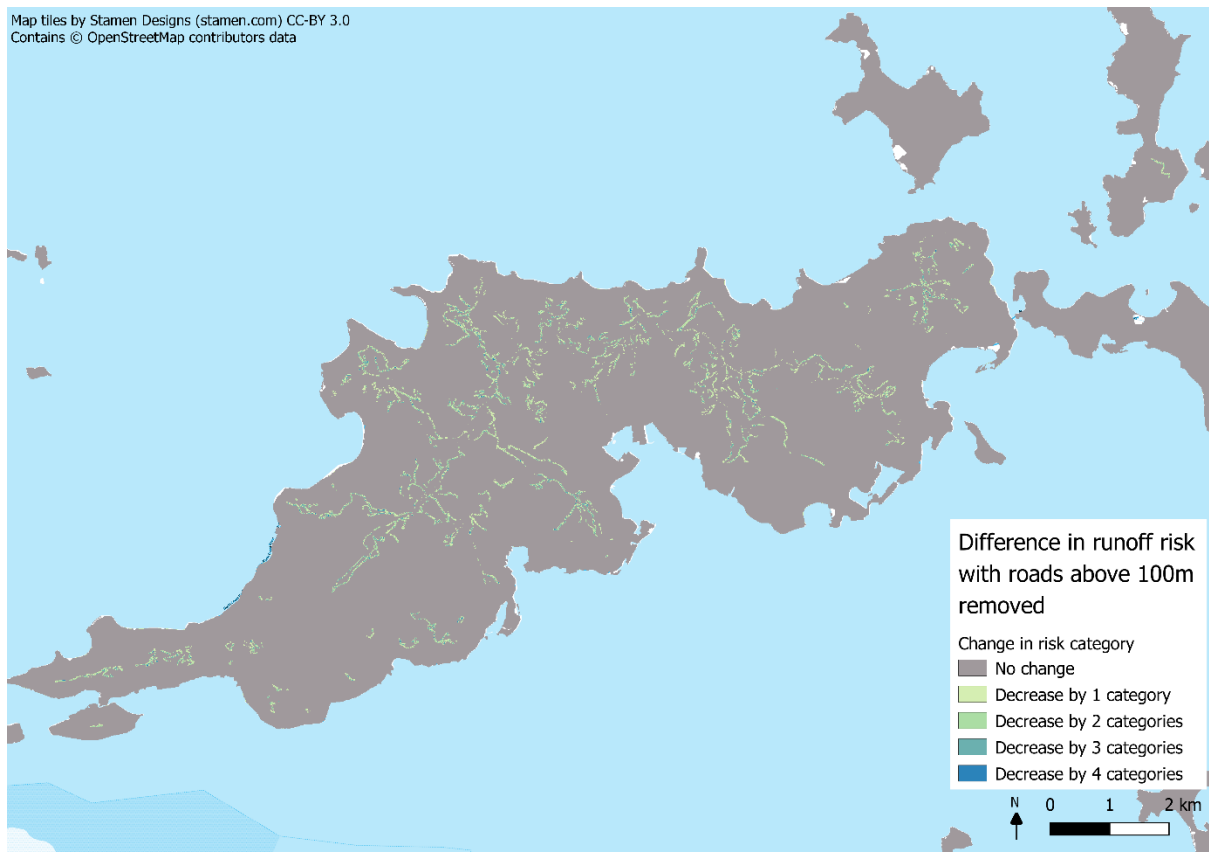


**Figure 24:** Natural Capital Scenario 2 where roads above 100m elevation were removed.

### 7.2.3 Expand urban areas

In this scenario, the urban areas were buffered by 10m to simulate urban expansion on the islands. Eighteen percent (18%) of the total areas on the islands experienced a negative change in flood risk category. Half of these showed only a slightly greater risk by moving up one category, e.g. Moderate to High risk, whereas 29% had an increase in risk of either Low to Very High or Very Low to Very High. Figure 25 shows where urban expansion could be most detrimental to the populated regions on the Virgin Gorda and around the airport of Beef Island and the northern tip of Tortola.

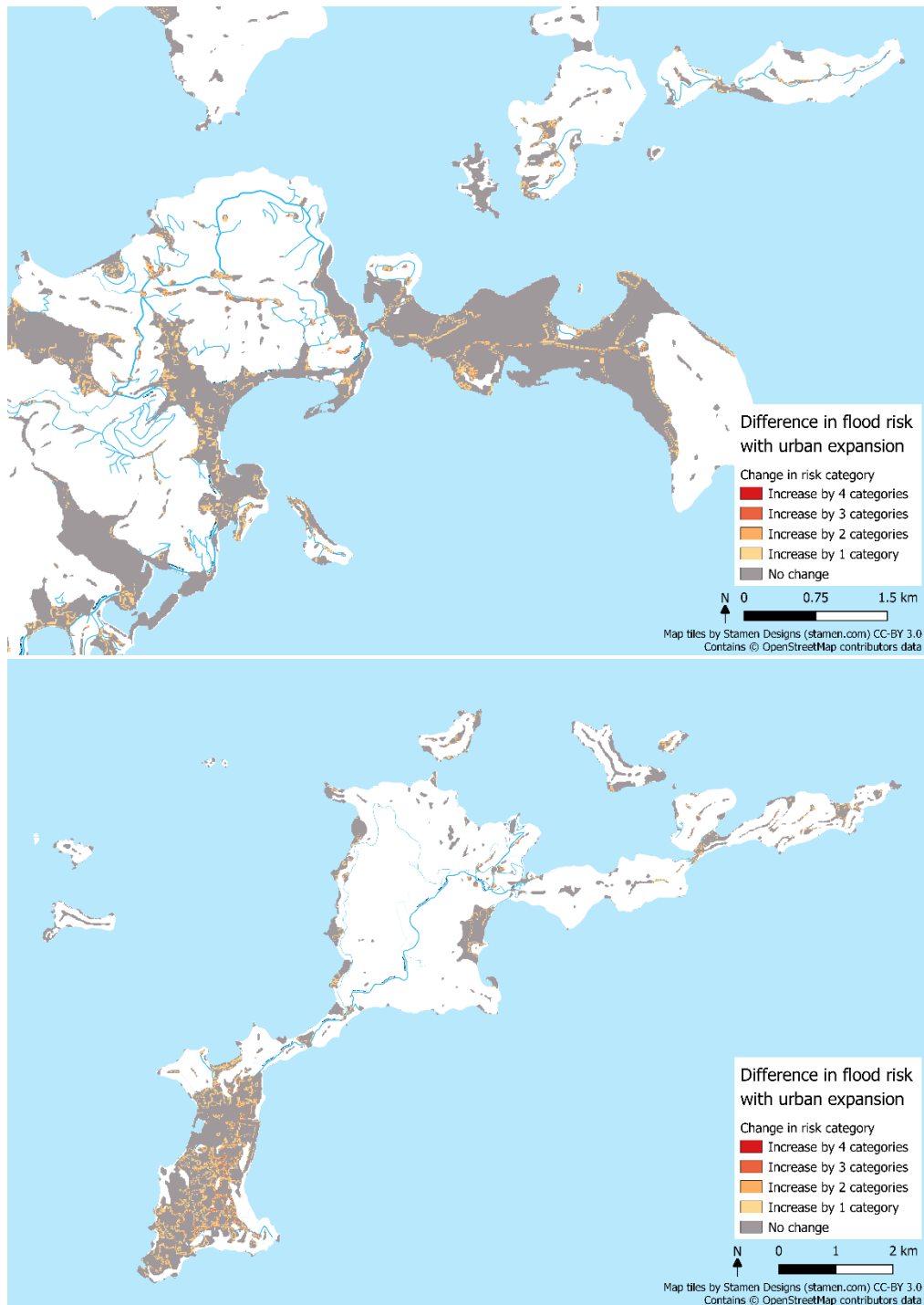


**Figure 25:** Predicted change in damage from flood risk under natural capital scenario 3, where urban areas were expanded by 10m. Top: Beef Island and northern Tortola; bottom: Virgin Gorda.

It should be noted that running the same scenario analyses under tropical storm conditions results in similar levels of change in risk. For instance, in scenario 5 (Section 7.2.2), 45% of the areas where runoff risk was reduced experienced a reduction in risk by 1 category and 42% reduced risk by 2 categories under tropical storm conditions, compared to 50% and 33% respectively under the category 3 storm conditions (results not shown). This demonstrates that for lower severity storms, there are greater proportional gains from the flood risk prevention properties of certain habitats than there are for the most severe storms.

## 8 Limitations and Next Steps

The inland flooding and storm surge models developed for the BVI provide a fast and repeatable workflow, which is fully automated using open-source tools and minimal data layers. The models can be run at high spatial resolutions (depending upon data availability) and the outputs provide an indication of the areas likely to experience high levels of risk of damage given different storm paths and severities. The inland flooding model predicts the risk of likely damage from runoff and flooding due to rainfall during extreme weather events, whereas the storm surge model predicts the risk posed by surge to both the terrestrial and marine environments.

These risk-based models were developed with the needs of the UK Overseas Territories in mind. The models have been designed to aid in the considerations of nature-based solutions and land use and are not intended to precisely predict actual flood areas. Data for the islands are often limited therefore, a risk-based approach was chosen over available hydrological models, which are more complex requiring a greater input of data and expertise to run the models and are often behind paywalls or unavailable to the public. Taking this approach has meant that our models do not use complex surface water algorithms to calculate hydrological flows, and so a lot of the intricacies of the water's movement and depth are not described. For instance, the inland flooding model does not capture hydrological pathways such as infiltration and throughflow, or the volume of surface water present, therefore importantly it cannot describe the depth of flood water during the storm event. For this, more complex modelling would be required, whereas our approach gives a fast indication of where areas of damage are more likely to occur. The model also does not consider ground saturation prior to the storm event, which is a key factor in determining the damage from inland flooding and the amounts of runoff waters being generated. This was evident in the case of Hurricane Maria where the islands experienced high precipitation levels a week after Hurricane Irma also struck the region (NOAA NHC 2020c). The inland flooding model can however be used to model how the degradation or removal of a habitat after such an event might change likely flooding risk. This is through the incorporation of the runoff conversion factors, which can be altered to assess predictions under these changed scenarios. These factors were established from studies using hydrological models in catchments in the UK (Perks *et al.* 2017), and then adapted to the habitats in the BVI. This is a source of error which could be informed by local data to help improve associated values for each habitat class. Another limitation of the method comes where the predicted flooding zones were restricted to a threshold slope and elevation. This was determined through similar methods used in the literature, however for the BVI the reality of this may be to exceed our estimated thresholds during storm events.

Similarly, the storm surge model is not a hydrological model, and applies a cost distance analysis to assess the likely risk of flood damage caused by storm surge, rather than modelling the actual movement of water, hydrological effects such as wave setup (World Meteorological Organization 2011), or the volume or depth of water inundating the land. The model makes several assumptions regarding the importance of key storm attenuating and propagating factors and assigns weighting values to these based upon a sensitivity analysis. The models were evaluated against the damage lines produced by Williams *et al.* (2018) as part of their vulnerability assessment of the BVI, but these damage lines were derived only after both Hurricanes Irma and Maria had damaged the islands, and are, undoubtedly, a result of a combination of factors (e.g. wind and wave damage) beyond storm surge. While our comparison of these damage lines against the modelled outputs for Hurricane Irma gives an indication of whether the model could correctly predict flooded areas as under risk, as these lines were capturing flooding after two storm events this comparison was not ideal for validation. The sensitivity analysis itself only tested a limited number of values for scaling factors, and the nature of the analysis favours over-estimation of risk and will therefore work

to minimise the weight of attenuating factors such as elevation and slope. Additionally, the scaling factor describing the change in cost with storm category is arbitrary and follows a linear pattern, which may not be representative of how flooding risk scales with increasing storm severity. In terms of the cost values themselves, due to a lack of local observations the Manning's n coefficient values were based on studies from the US and Japan, therefore some inaccuracy is introduced in assigning these values to the observed habitat classes present in the BVI. There are also some erroneous changes and sudden spikes in elevation and slope in a small number of areas where multiple bathymetry and elevation data layers of different resolutions are resampled and overlaid together. This approach was taken in order to cover as much of the islands as possible with high resolution data, to get the most accurate predictions for changes in slope and elevation across the landscape.

As well as inaccuracies in the data, the method applying the cost distance analysis cannot account for a number of key attributes effecting the risk from surge, including the size of the storm, or fully capture the effects of changes in pressure, wind energy and windspeed with increasing storm severity. Such changes in storm severity are currently accounted for by changes in the cost landscape over which the modelled storm moves, and by assuming that increasing storm category means increasing severity in other ways. However, the effects of fetch distance, and the distance travelled over the continental shelf, are constant with storm category although vary slightly with the extent of the modelled area. Furthermore, while the effects of fetch and shelf distance act in the same direction as storm surge, the cost distance analysis is calculated from the storm's path, thus the costs experienced in a cell may not represent those directly storm-ward of the cell in the direction of travel of the waves, and therefore may be under or overestimated in some regions. Additionally, the risk levels are heavily influenced by the distance of areas from the storm path, as such it is likely that the risk of areas further away from the path of the storm would be underpredicted. Given the complexity of storm surge, and the myriad factors that contribute to its severity, it is however unsurprising that a simple model as presented here is unable to capture the more nuanced elements of the phenomenon. A further example of this can be seen in Figure 26 (below). Previous studies of storm surge have observed that enclosed areas such as bays or estuaries can cause a water funnelling effect (e.g. As-Salek 1998), which acts to enhance the magnitude of surge in areas such those pictured (in this case Road Town, Tortola). However, this simple model is unable to capture such dynamics, and as a result is likely to be underestimating risk in such areas, a probable reason that areas observed as damaged were not classified as Moderate risk or greater by the model.

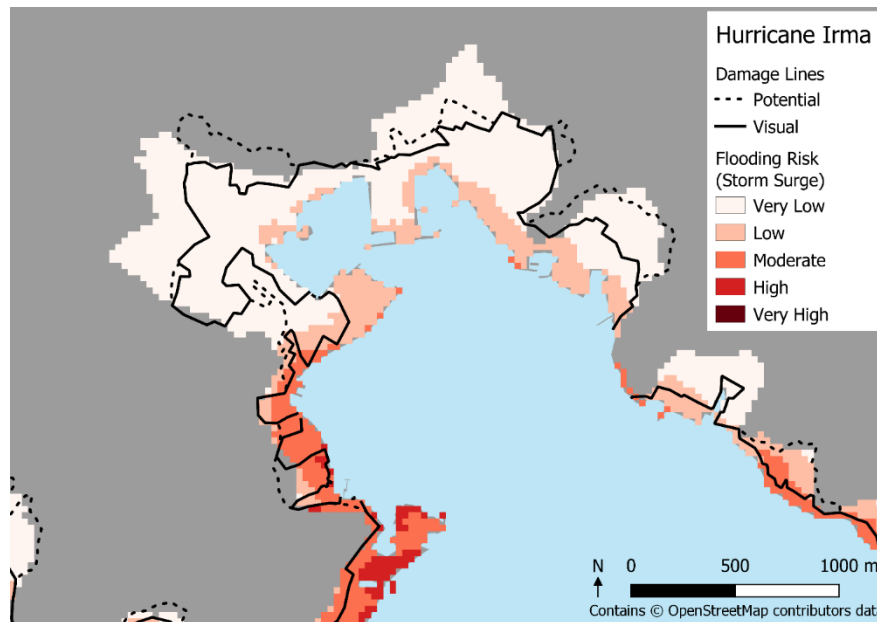


**Figure 26:** Modelled risk for Road Town, Tortola, under Hurricane Irma. Misalignment between modelled and observed risk is a result of a number of factors, including a lack of representation of funnelling in the model.

The models however were not designed to replace any large-scale complex modelling used for disaster risk monitoring or to estimate actual storm damage or risk to life. The purpose of these models is to assess relative risk to the islands from flooding by rain or storm surge and demonstrate how the natural environment and nature-based solutions can play a role to storm resilience.

## 9 References

- Arnold, J.G., Kiniry, J.R., Srinivasan, R., Williams, J.R., Haney, E.B. & Neitsch, S.L. 2012. SWAT Water Assessment Tool: Input/Output Documentation Version 2012. Texas Water Resources Institute TR-439. Available from: <https://swat.tamu.edu/media/69296/swat-iodocumentation-2012.pdf> [Accessed 07/01/2019]
- Asher Greenberg, J. & Mattiuzzi, M 2018. Package 'gdalUtils'. Wrapper for the Geospatial Data Abstraction Library (GDAL). Version 2.0.1.14. Available from: <https://cran.r-project.org/web/packages/gdalUtils/gdalUtils.pdf> [Accessed 15/10/2019].
- As-Salek, J.A. 1998. Coastal Trapping and Funneling Effects on Storm Surges in the Meghna Estuary in Relation to Cyclones Hitting Noakhali–Cox’s Bazar Coast of Bangladesh. *American Meteorological Society*, **28**:227-249
- Barbier, E.B., Georgiou, I.Y., Enchelmeyer, B. & Reed, D.J. 2013. The Value of Wetlands in Protecting Southeast Louisiana from Hurricane Storm Surges. *PLoS ONE* **8**:e58715
- Bartleson, R.D. 2004. Interactions of seagrass beds and the water column: effects of bed size and hydrodynamics. PhD Thesis, University of Maryland
- Beven, K. & Freer, J. 2001. A dynamic TOPMODEL. *Hydrological Processes* **15**(10): 1993-2011. doi: <https://doi.org/10.1002/hyp.252>
- Bray, S., Carter, C., Cunningham, E. & Fawcett, C. 2019. An assessment of the value of natural capital in the protective service against coastal and inland flooding in the UK Overseas Territory of the British Virgin Islands. *Natural Capital in the UK’s Overseas Territories: Report Series – Supplementary Report (Caribbean Region)*. Contracted report to JNCC for The Natural Capital in the Caribbean and South Atlantic Overseas Territories: Valuation, Vulnerability and Monitoring change project. <https://hub.jncc.gov.uk/assets/c8e46472-2bfc-4a70-b6e8-573f1807c158>
- Brenning, A., Bangs, D., Becker, M., Schratx, P. & Polakowski, F. 2018. RSAGA: SAGA Geoprocessing and Terrain Analysis. Version 1.3.0. Available from: <https://cran.r-project.org/web/packages/RSAGA/index.html> [Accessed. 13/09/2018].
- Chang, W., Borges, B., RStudio; Almasaeed Studio & Adobe Systems Incorporated. 2018. Package 'shinydashboard'. Create dashboards with 'Shiny'. Available from: <https://cran.r-project.org/web/packages/shinydashboard/shinydashboard.pdf> [Accessed 19/03/2020].
- Cialone, M.A. & Smith, J. McK. 2007. Wave transformation modeling with bottom friction applied to southeast Oahu reefs. 10th International Workshop on Wave Hindcasting and Forecasting & Coastal Hazard Assessment. 12p.
- Conrad, O. 2007. SAGA-GIS Module Library Documentation (v2.1.4) Module GDAL: Import Raster. GDAL Version: 1.7.3. Available from: [http://www.saga-gis.org/saga\\_tool\\_doc/2.1.4/io\\_gdal\\_0.html](http://www.saga-gis.org/saga_tool_doc/2.1.4/io_gdal_0.html) [Accessed 15/09/2019].
- Conrad, O., Bechtel, B., Bock, M., Dietrich, H., Fischer, E., Gerlitz, L., Wehberg, J., Wichmann, V. & Böhner, J. 2015. System for Automated Geoscientific Analyses (SAGA) v. 2.1.4, *Geosci. Model Dev.*, **8**, 1991-2007, doi:10.5194/gmd-8-1991-2015.
- Dasgupta, S., Islam, M.S., Huq, M., Huque Khan, Z. & Hasib, M.R. 2019. Quantifying the

protective capacity of mangroves from storm surges in coastal Bangladesh. PLoS ONE **14**(3): e0214079. <https://doi.org/10.1371/journal.pone.0214079>

Department of Disaster Management, British Virgin Islands. 2019. Department of Disaster Management, British Virgin Islands. Available from: <https://www.bviddm.com> [Accessed 15/10/2019].

Ellis, J.T. & Sherman, D.J. 2015. Perspectives on Coastal and Marine Hazards and Disasters. Coastal and Marine Hazards, Risks, and Disasters, p1-13

Environmental Systems Research Institute. 2020. ArcGIS. [www.arcgis.com/](http://www.arcgis.com/)

Fairfield, J. & Leymarie, P. 1991. Drainage networks from grid digital elevation models. Water Resources Research **27**: 709–717.

Finlayson, D. 2005. Waves Toolbox for ArcGIS 10.x.CC-BY-NC-SA 3.0

GEBCO Compilation Group. 2019. GEBCO 2019 Grid (doi:10.5285/836f016a-33be-6ddc-e053-6c86abc0788e)

Getahun, Y.S. & Gebre, S.L. 2015. Flood Hazard Assessment and Mapping of Flood Inundation Area of the Awash River Basin in Ethiopia using GIS and HEC-GeoRAS/HEC-RAS Model. Journal of Civil & Environmental Engineering **5**: 179 doi:10.4172/2165-784X.1000179

Government of the Virgin Islands. 2017. Situation Report 003 (Final). 15p. Available online: <http://bviddm.wpengine.com/wp-content/uploads/2017/10/Irma-SITRIP-3-Revised-1.pdf>

GRASS Development Team. 2019. Geographic Resources Analysis Support System (GRASS) Software, Version 7.6.0. Open Source Geospatial Foundation. <https://grass.osgeo.org>

Hamilton, C. 2019. Shape Tools 3.3.10. Available online: <https://plugins.qgis.org/plugins/shapetools/>

Hijmans, R.J. 2019. raster: Geographic Data Analysis and Modeling. R package version 2.9-5. <https://CRAN.R-project.org/package=raster>

Hijmans, R.J., Cameron, S.E., Parra, J.L., Jones, P.G. & Jarvis, A. 2005. Very high resolution interpolated climate surfaces for global land areas. International Journal of Climatology **25**: 1965-1978.

Hojati, M. & Mokarram, M. 2016 Determination of a topographic wetness index using high resolution digital elevation models. European Journal of Geography **7**(4):41-52.

Horn, B.K.P. 1981. Hill shading and the reflectance map. Proceedings of the IEEE **69**:14-47

Huffman, G., Bolvin, D., Braithwaite, D., Hsu, K., Joyce, R. & Xie, P. 2014. Integrated Multi-satellitE Retrievals for GPM (IMERG), version 4.4. NASA's Precipitation Processing Center accessed 31 March 2015, <ftp://arthurhou.pps.eosdis.nasa.gov/gpmdata/>

Irish, J.L., Resio, D.T. & Ratcliff, J.J. 2008. The influence of storm size on hurricane surge. Journal of Physical Oceanography, **38**:2003-2013

ISRIC. 2019. Harmonized continental SOTER-derived database (SOTWIS). Available from: <https://www.isric.org/index.php/projects/harmonized-continental-soter-derived-database-sotwis> [Accessed 13/09/2019].

Jelesnianski, C.P., Chen, J. & Shaffer, W.A. 1992. SLOSH: Sea, Lake, and Overland Surges from Hurricanes. NOAA Technical Report NWS 48, Silver Spring, MD. 77p.

Kennaway, T. Helmer, E., Lefsky, M., Brandeis, T. & Sherrill, K. 2008. Mapping land cover and estimating forest structure using satellite imagery and coarse resolution lidar in the Virgin Islands. *Journal of Applied Remote Sensing* **2**: 023551

Kraines, S.B., Yanagi, T., Isobe, M. & Komiyama, H. 1998. Wind-wave driven circulation on the coral reef at Bora Bay, Miyako Island. *Coral Reefs*, **17**:133-143

Lane, S.N., Brookes, C.J., Kirkby, M.J. & Holden, J. 2004. A network-index-based version of TOPMODEL for use with high-resolution digital topographic data. *Hydrological processes* **18**: 191-201.

Lim, Y.K., Schubert, S.D., Kovach, R., Molod, A.M. & Pawson, S. 2018. The Roles of Climate Change and Climate Variability in the 2017 Atlantic Hurricane Season. *Scientific Reports*, **8**:16172

Loder, N.M., Irish, J.L., Cialone, M.A. & Wamsley, T.V. 2009. Sensitivity of hurricane surge to morphological parameters of coastal wetlands. *Estuarine, Coastal and Shelf Science*, **84**:625-636

Mattocks, C., Forbes, C. & Ran, L. 2006. Design and Implementation of a Real-Time Storm Surge and Flood Forecasting Capability for the State of North Carolina. UNC-CEP Technical Report. Carolina Environmental Program, University of North Carolina, Chapel Hill, North Carolina.

Möller, I., Kudella, M., Rupprecht, F., Spencer, T., Paul, M., van Wesenbeeck, B.K., Wolters, G., Jensen, K. *et al.* 2014. Wave attenuation over coastal salt marshes under storm surge conditions. *Nature Geoscience* **7**:727-731

Natural England. 2015. SCIMAP Sediment risk mapping for designated Site Catchments. Improvement Programme for England's Natura 2000 Sites (IPENS) – Planning for the Future IPENS008b. Westcountry Rivers Ltd. Cornwall

NOAA NHC. 2020a. National Hurricane Center (NHC) and Central Pacific Hurricane Center (CPHC), National Oceanic and Atmospheric Administration (NOAA): Storm surge frequently asked questions. Available online: <https://www.nhc.noaa.gov/surge/faq.php>

NOAA NHC. 2020b. National Hurricane Center (NHC) and Central Pacific Hurricane Center (CPHC), National Oceanic and Atmospheric Administration (NOAA): Sea, Lake, and Overland Surges from Hurricanes (SLOSH). Available online: <https://www.nhc.noaa.gov/surge/slosh.php>

NOAA NHC. 2020c. National Hurricane Center (NHC) and Central Pacific Hurricane Center (CPHC), National Oceanic and Atmospheric Administration (NOAA): 2017 Atlantic Hurricane Season. Available online: <https://www.nhc.noaa.gov/data/tcr/index.php?season=2017&basin=atl> [Accessed: 04/11/2019]

NOAA NHC. 2020d. National Hurricane Center (NHC) and Central Pacific Hurricane Center (CPHC), National Oceanic and Atmospheric Administration (NOAA): Saffir-Simpson hurricane wind scale. Available online: <https://www.nhc.noaa.gov/aboutsshws.php>

O'Callaghan, J. & Mark, D. 1984. The extraction of drainage networks from digital elevation data, *Computer Vision, Graphics and Image Processing* **28**: 323–344.

OpenStreetMap. 2019. OpenStreetMap. Available from: <https://www.openstreetmap.org/> [Accessed 02/10/2019].

Pasch, R.J., Penny, A.B. & Berg, R. 2019. National Hurricane Center Tropical Cyclone Report: Hurricane Maria (AL152017). Available from: [https://www.nhc.noaa.gov/data/tcr/AL152017\\_Maria.pdf](https://www.nhc.noaa.gov/data/tcr/AL152017_Maria.pdf) [Accessed 19/03/2020].

Perks, M.T., Warburton, J., Bracken, L.J., Reaney, S.M., Emery, S.B. & Hirst, S. 2017. Use of spatially distributed time-integrated sediment sampling networks and distributed fine sediment modelling to inform catchment management. *Journal of Environmental Management* **202**: 469-478.

Perks, M.T., Warbuton, J., Bracken, L.J., Reaney, S.M., Emery, S.B. & Hirst, S. 2017. Use of spatially distributed time-integrated sediment sampling networks and distributed fine sediment modelling to inform catchment management. *Journal of Environmental Management* **202**: 469-478.

Pinet, P.R. 2003. *Invitation to Oceanography*. Jones & Bartlett Learning, p528

Pinsky, M.L., Guannel, G. & Arkema, K.K. (2013) Quantifying wave attenuation to inform coastal habitat conservation. *Ecosphere*, **4**:95

Prager, E.J. 1991. Numerical simulation of circulation in a Caribbean-type backreef lagoon. *Coral Reefs*, **10**:177–182

QGIS Development Team. 2018. QGIS Geographic Information System v3.4.5. Open Source Geospatial Foundation Project. <http://qgis.osgeo.org>

R Core Team. 2019. *R: A Language and Environment for Statistical Computing*. Vienna, Austria. Available from: <https://www.R-project.org/>

Rappaport, E.N. 2014. Fatalities in the United States from Atlantic tropical cyclones: new data and interpretation. *Bulletin of the American Meteorological Society*, **March 2014**:341-346

Reaney, S. & Pearson, C. 2019. Spatial targeting of natural flood risk management within large river catchments: A nested approach of SCIMAP-Flood and CRUM3. Department of Geography, Durham University, Durham.

Reaney, S., Lane, S.N., Heathwait, A.L. & Dugdale, L.J. 2011. Risk-based modelling of diffuse land use impacts from rural landscapes upon salmonid fry abundance. *Ecological Modelling* **222** (4): 1016-1029.

Resio, D.T. & Westerink, J.J. 2008. Modelling the physics of storm surges. *Physics Today*, **September 2008**:33-38

Rohweder, J. 2012. *Waves Toolbox for ArcGIS 10.x – 2012 Update*. CC-BY-NC-SA 3.0

Rohweder, J., Rogala, J.T., Johnson, B.L., Anderson, D., Clark, S., Chamberlin, F., Potter, D. & Runyon, K. 2012. Application of Wind Fetch and Wave Models for Habitat Rehabilitation and Enhancement Projects – 2012 Update. Contract report prepared for U.S. Army Corps of Engineers' Upper Mississippi River Restoration – Environmental Management Program. 52p.

Rosman, J.H. & Hench, J.L. 2011. A framework for understanding drag parameterizations for coral reefs. *Journal of Geophysical Research*, **116**:1-15

SCIMAP. 2017. SCIMAP – Diffuse Pollution Risk Mapping: A framework for modelling and mapping diffuse pollution risk across landscapes. Available from: <http://www.scimap.org.uk/scimap-fine-sediment/> [Accessed 16/09/2019].

Spalding, M., Mclvor, A., Tonneijck, F.H., Tol, S. & van Eijk, P. 2014 Mangroves for coastal defence. Guidelines for coastal managers & policy makers. Published by Wetlands International and The Nature Conservancy. 42 pp.

Tarboton, D.G. 1997. A new method for the determination of flow directions and upslope areas in grid digital elevation models, *Water Resources Research* **33**: 309–319.

Toffoli, A. & Bitner-Gregersen, E.M. 2017. Types of Ocean Surface Waves, Wave Classification. *Encyclopedia of Maritime and Offshore Engineering*, 8p.

UNDP. 2019. Regional overview: Impact of Hurricanes Irma and Maria. Conference Supporting Document. 21 Nov 2017. Available from: <https://reliefweb.int/report/dominica/regional-overview-impact-hurricanes-irma-and-maria> [Accessed: 30/07/2020].

University of the West Indies. 2017. Hurricane Irma and Maria 2017. Available online: <http://www.uwi.edu/ekacdm/node/68>

Wamsley, T.V., Cialone, M.A., Smith, J.M., Atkinson, J.H. & Rosati, J.D. 2010. The potential of wetlands in reducing storm surge. *Ocean Engineering* **37**:59-68

Wang, L. & Liu, H. 2006. An efficient method for identifying and filling surface depressions in digital elevation models for hydrologic analysis and modelling. *Int. J. Geogr. Inf. Sci.*, **20**, 193– 213, 2006.

Westerink, J.J., Luettich, R.A., Feyen, J.C., Atkinson, J.H., Dawson, C., Roberts, H.J., Powell, M.D., Dunion, J.P., Kubatko, E.J. & Pourtaheri, H. 2006. A basin to channel scale unstructured grid hurricane storm surge model applied to Southern Louisiana. *Monthly Weather Review*, **136** (3): 833–864.

Williams, J., Medcalf, K., Pike, S., Naumann, E.K. & van Zanten, B. *et al.* 2017. Using radar-based terrain mapping to model the vulnerability of 5 UK OTs. *Natural Capital in the UK's Overseas Territories: Report Series – Supplementary Report (Caribbean Region)*. Contracted report to JNCC for The Natural Capital in the Caribbean and South Atlantic Overseas Territories: Valuation, Vulnerability and Monitoring change project. . <https://hub.jncc.gov.uk/assets/9cf14760-61b2-4b06-a290-4a4f6d3bfb8b>

Williams, J., Medcalf, K., Rugg, J. & Pike, S. 2018. Assess and validate the vulnerability mapping of the UK's OTs of Anguilla and BVI to natural hazards, and the value of natural capital in mitigating impacts. *Natural Capital in the UK's Overseas Territories: Report Series – Supplementary Report (Caribbean Region)*. Contracted report to JNCC for The Natural Capital in the Caribbean and South Atlantic Overseas Territories: Valuation, Vulnerability

and Monitoring change project. <https://hub.jncc.gov.uk/assets/032a88e6-a264-46c2-a2b1-3aa49d11e0a7>.

Windfinder. 2020. Wind & weather statistics for Beef Isl./Tortola. Available online: [https://www.windfinder.com/windstatistics/beef\\_isl\\_tortola](https://www.windfinder.com/windstatistics/beef_isl_tortola) [Accessed: 11/11/2019]

World Meteorological Organization. 2011. Guide to Storm Surge Forecasting. WMO-No. 1076, Geneva, Switzerland. 120p.

Xiao, C., Zhang, K. & Shen, J. 2006 CEST: A three-dimensional coastal and estuarine storm tide model. Miami, Florida: International Hurricane Research Center, Florida International University, 20p.

Zevenbergen, L.W. & Thorne, C.R. 1987. Quantitative analysis of land surface topography. *Earth Surface Processes and Landforms*. **12**: 47-56.

Zhang, K., Li, Y., Liu, H., Rhome, J. & Forbes, C. 2013. Transition of the Coastal and Estuarine Storm Tide Model to an Operational Storm Surge Forecast Model: A Case Study of the Florida Coast. *Weather and Forecasting* **28**:1019-1037.

Zhang, K., Xiao, C. & Shen, J. 2008. Comparison of the CEST and SLOSH models for storm surge flooding. *Journal of Coastal Research*, **24**:489-499

Zhu, D., Ren, Q., Xuan, Y., Chen, Y. & Cluckie, I.D. 2013. An effective depression filling algorithm for DEM-based 2D surface flow modelling. *Hydrology and Earth System Sciences* **17**, 495-505